

1 Decadal trends (2013-2023) in PM₁₀ sources and oxidative 2 potential at a European urban supersite (Grenoble, France)

3 Vy Ngoc Thuy Dinh¹, Jean-Luc Jaffrezo¹, Pamela A. Dominutti¹, Rhabira Elazzouzi¹, Sophie
4 Darfeuil¹, Céline Voiron¹, Anouk Marsal¹, Stéphane Socquet², Gladys Mary², Julie Cozic²,
5 Catherine Coulaud¹, Marc Durif^{3,4}, Olivier Favez^{3,4}, Gaëlle Uzu¹

6 ¹ Université Grenoble Alpes, CNRS, IRD, INP-G, INRAE, IGE (UMR 5001), 38000 Grenoble, France

7 ²Atmo Auvergne-Rhône-Alpes (Atmo AuRA), 69500 Bron, France

8 ³ INERIS, Parc Technologique Alata, BP 2, 60550 Verneuil-en-Halatte, France

9 ⁴ Laboratoire central de surveillance de la qualité de l'air (LCSQA), 60550 Verneuil-en-Halatte, France

10 Correspondence to: Gaëlle Uzu gaelle.uzu@univ-grenoble-alpes.fr

12 Abstract

13 The identification of particulate matter (PM) sources and the quantification of their contribution to the urban
14 environment is a necessary input for policymakers to reduce the air pollution impacts. The association between
15 the PM sources and the oxidative potential (OP) is also a key indicator for evaluating the ability of PM sources to
16 induce *in-vivo* oxidative stress and lead to adverse health effects, which becomes an emerging metric in the
17 Directive on ambient air quality (22024/2881/EU). Most studies in Europe have focused on PM and OP sources
18 in the short term, for only 1 or 2 years. However, the efficiency of reduction policies, trends, and epidemiological
19 impacts cannot be properly evaluated with such short-term studies due to a lack of statistical robustness. Here,
20 long-term PM₁₀ filter sampling at the Grenoble (France) urban background supersite and detailed chemical
21 analyses were used to investigate decadal trends of the main PM sources and related OP metrics. Positive matrix
22 factorization (PMF) analyses were conducted on the corresponding 11-year dataset (Jan 2013 to May 2023, n =
23 1570), enlightening the contributions of 10 PM sources: mineral dust, sulfate-rich, primary traffic, biomass
24 burning, primary biogenic, nitrate-rich, MSA-rich, aged sea salt, industrial and chloride-rich. The stability of the
25 chemical profile of these sources was validated by comparison with the profiles retrieved from shorter-term (3
26 years) successive PMF analyses. A Seasonal-Trend using LOESS decomposition was then applied to evaluate the
27 trends of these PM₁₀ sources, which revealed a substantial decrease in PM₁₀ (-0.73 µg m⁻³ yr⁻¹) as well as that of
28 many of the PM₁₀ sources. Specifically, negative trends for primary traffic and biomass burning sources are
29 detected, with a reduction of 0.30 and 0.11 µg m⁻³ yr⁻¹, respectively. The OP PM₁₀ source apportionment in 11
30 years confirmed the high redox activity of the anthropogenic sources, including biomass burning, industrial, and
31 primary traffic. Eventually, downward trends were also observed for OP_{AA} and OP_{DTT}, mainly driven by the
32 reduction of residential heating and transport emissions, respectively.

33 Keywords: PM₁₀ source apportionment, OP PM₁₀ source apportionment, long-term trend, Positive matrix
34 factorization.

35 1. Introduction

36 Particulate matter (PM) is the main atmospheric pollutant that significantly impacts human health, climate, and
37 the environment (Fuzzi et al., 2015; Grantz et al., 2003; Pope and Dockery, 2006), which is emitted directly or

38 formed through complex processes in the atmosphere from natural and anthropogenic gaseous precursors. The
39 identification of PM sources is important to investigate their composition, contribution, and evolution, which is
40 one necessary input for policymakers to apply strategies in reducing their impact. There are various methodologies
41 to identify these sources, where receptor models are widely used to perform source apportionment (SA) due to
42 their flexibility and performance. Positive Matrix factorization (PMF) is one of the most popular among these
43 receptor models, as it has been developed to allow SA analysis without any prior information other than the
44 measurement and uncertainty input matrices (Hopke, 2016). Scores of studies using PMF have been applied in
45 different typologies of sites over the last 15 years, with urban areas being the most common (Hopke et al., 2020;
46 Viana et al., 2008).

47 The adverse health effects of PM can be assessed through different pathways, one of which uses the concept of
48 oxidative stress within the lung (Pope and Dockery, 2006). PM has the ability to generate reactive oxygen species
49 (ROS), which can cause an imbalance with antioxidants in the lungs, eventually causing oxidative stress. This
50 capacity is evaluated as the oxidative potential (OP) of PM (Ayres et al., 2008; Li et al., 2008; Lodovici and
51 Bigagli, 2011; Mudway et al., 2020; Nelin et al., 2012; Rao et al., 2018). The redox activity of PM is mainly
52 dependent on their compositions; nevertheless, the correlation between individual components of PM and OP is
53 probably not the best approach for understanding the impact of ambient PM because of their complex mixture
54 preventing the quantification of all components of interest (Borlaza, 2021; Calas et al., 2018; Weber et al., 2018).
55 Therefore, the relationship between OP and PM sources has been investigated as a more holistic approach (Bates
56 et al., 2018; Dominutti et al., 2023; Weber et al., 2021). The implementation steps of such an approach can include,
57 first, a PM source apportionment (SA) (usually using PMF), allowing the identification of PM sources and their
58 contribution to PM. Then, the relationship between OP and PM sources is investigated by performing some
59 regression techniques, potentially including linear and non-linear ones (Ngoc Thuy et al., 2024).

60 The OP of PM is becoming an emerging metric for the European regulation on air quality, included in the new
61 European Air Quality Directive (Directive (EU) 2024/2881) as a recommended measurement at super sites in each
62 member state in order to improve the knowledge about the variability of the OP and eventually allow the
63 connections with epidemiological studies. Most previous studies have focused on PM and OP sources over a
64 relatively short period, typically less than 1 or 2 years (Borlaza et al., 2022a; Pietrodangelo et al., 2024; Weber et
65 al., 2019). Such short-term studies assess the PM and OP sources as well as their contribution, providing
66 information on the intrinsic OP of PM sources, allowing for the development of OP modeling (Daellenbach et al.,
67 2020; Vida et al., 2024) and eventually designing some public policies (Borlaza, 2021). However, long-term series
68 are needed both for evaluating the efficiency of such reduction policies in connection with the evolution of
69 contributions from sources and also for implementing epidemiological studies (Borlaza-Lacoste et al., 2024).

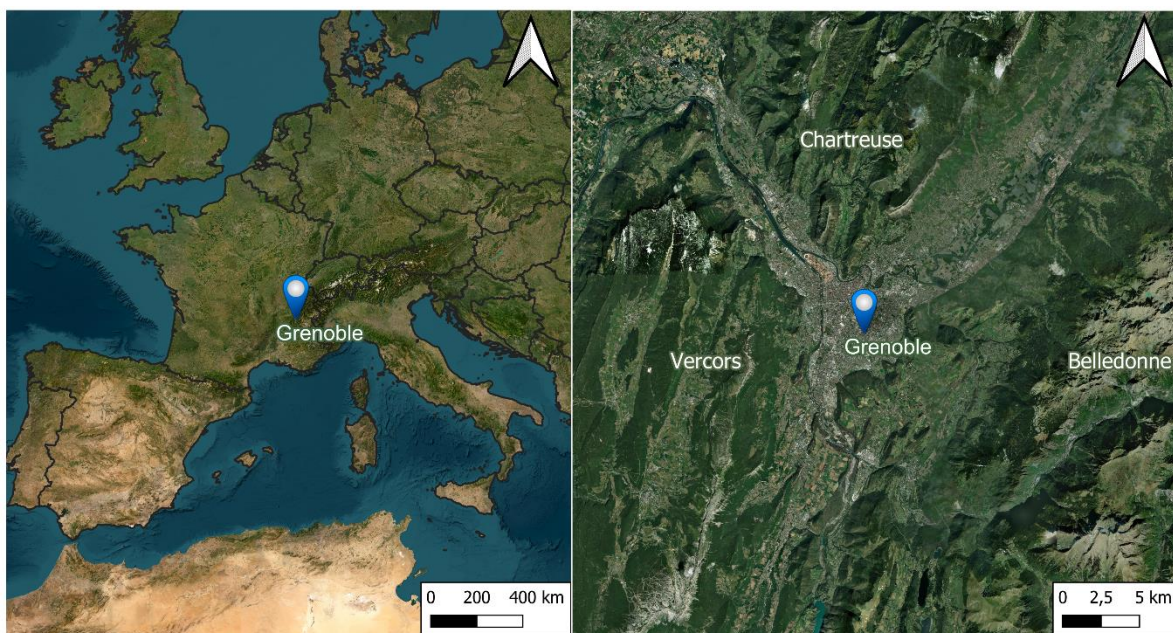
70 The present study is based on a long-term measurement program conducted in the city of Grenoble (France),
71 resulting from a sustained collaboration between the local network (Atmo AuRA), the French Reference
72 Laboratory for Air Quality Monitoring (LCSQA), and the Institute of Environmental Geosciences (IGE) to
73 investigate long-term evolution of PM₁₀ sources and OP in the PM₁₀ as well as their tendencies in the urban
74 background of the city. Here, we assessed these source contributions from daily ambient PM₁₀ samples obtained
75 from 2013 to 2023 (n= 1570) using the EPA PMF model at this site selected as one of the French urban supersites
76 for the new EU 2024/2881 Air Quality Directive. The database was augmented using imputation techniques in
77 order to fill some of the gaps in the data, relative to metallic trace elements. Since PMF is rarely applied to such

78 a long-term database, several evaluations of the validity of solutions were also implemented. The PMF-derived
79 PM₁₀ sources were then used to perform OP SA from 2013 to 2022 (n=1570). The trend of PM₁₀ concentration,
80 of the PM₁₀ sources, and the OP measurements are eventually discussed in relation to several potential factors of
81 influence.

82 **2. Methodology**

83 **2.1. Sampling site**

84 PM₁₀ daily samples were collected at an urban background site (Grenoble - Les Frênes), in the southern area of
85 Grenoble, France (45°09'41" N, 5°44'07" E). This city is known as the French Alps' capital, sprawling over 18.13
86 km² with about 154,000 inhabitants in 2023, but nearly 500,000 within the larger urbanized area (about 15 km
87 radius). With an average altitude of about 200 masl, the city sits within a complex mountainous geomorphology
88 and is surrounded by three mountain massifs: Chartreuse, Vercors, and Belledonne (Figure 1). A pendular wind
89 regime between the three valleys of the basin regulates the ventilation of the atmosphere, with frequent thermal
90 inversion during cold periods, leading to the accumulation of pollutants. The air quality is monitored at several
91 sites in Grenoble by the regional agency (Atmo AuRA), including the urban background site of this study, which
92 is equipped with a large array of instruments. Particularly, the chemistry of PM₁₀ collected on filters has been
93 speciated at this site since 2008, within several programs, including the CARA program from the French Ministry
94 of Environment (Favez et al., 2021) and several research programs such as QAMECS (Borlaza et al., 2021), or
95 SOURCES (Weber et al., 2019). Many aspects of air quality in Grenoble were reported for this site, including the
96 characteristics of secondary anthropogenic PM fraction (Baduel et al., 2009, 2012; Favez et al., 2010; Tomaz et
97 al., 2016, 2017), of the biogenic PM components (Brighty et al., 2022; Samaké et al., 2019a, a), as well as the PM
98 OP (Borlaza, 2021; Dominutti et al., 2023; Weber et al., 2021). Several studies of one-year PM sources
99 apportionment were also performed in 2013 (Srivastava et al., 2018) and 2017-2018 (Borlaza et al., 2021). Despite
100 the difference in input data and periods of the studies, similar main sources of PM were quantified in both studies,
101 including residential heating, traffic, and secondary inorganic aerosol (SIA).



103 **Figure 1. The sampling site is located in the Southeast of France (left figure), surrounded by 3 mountains massifs**
104 **(Vercors, Chartreuse, and Belle donne). Background map: ESRI satellites.**

105 **2.2. Sampling and chemical analyses**

106 **2.2.1. PM₁₀ and their inorganic and organic composition**

107 The daily PM₁₀ sampling was performed every third day from 02/01/2013 to 28/05/2023, on 150 mm-diameter
108 quartz fibre filter (Tissu-quartz PALL QAT-UP 2500 diameter 150 mm) using high-volume samplers (Digitel
109 DA80, 30 m³ h⁻¹). A weekly PM₁₀ sampling was conducted during the same period using a low-volume sampler
110 (Partisol, 1 m³ h⁻¹) onto 47mm diameter quartz fibre filters (Tissuquartz PALL QAT-UP 2500 diameter 47 mm).
111 The processes of preparation, handling, and storing filters, in order to guarantee optimum quality for chemical
112 analyses were presented in Borlaza et al. (2021). Field blank filters were also collected (about 8-10% of the total
113 samples) to estimate the detection limits and evaluate the filter contamination during the overall handling and
114 analysis processes.

115 The daily PM₁₀ samples (n = 1570) and field blanks were analyzed for elemental carbon (EC) and organic carbon
116 (OC), major ions (Cl⁻, NO₃⁻, SO₄²⁻, Na⁺, NH₄⁺, K⁺, Mg²⁺, Ca²⁺), methanesulfonic acid (MSA), anhydrous sugar
117 and saccharides (levoglucosan, mannosan, arabitol, mannitol), and trace elements (As, Ba, Cd, Cr, Cu, Mn, Ni, Pb,
118 Sb, V, Zn). However, the concentrations of the daily trace elements were analyzed only in 3 periods, including:
119 (1) from January 2nd, 2013 to December 31st, 2013 (n = 122), (2) from February 28th, 2017 to March 13th, 2018
120 (n = 125), (3) from June 30th, 2020 to June 18th, 2021 (n=115). The weekly samples and blanks were analyzed
121 for trace metal concentrations for the whole sampling period (n = 842).

122 All analyses were previously described in detail (Borlaza et al., 2021). In brief, EC and OC analysis was performed
123 using a Sunset Lab analyser with the EUSAAR2 thermo-optical protocol. The eight major ionic components and
124 MSA were analyzed, after aqueous extraction of the filters using orbital shacking, by ionic chromatography using
125 an ICS3000 dual-channel chromatograph (Thermo-Fisher) with a CS16 column for cation analysis and an AS11
126 HC column for anion analysis. The anhydrous-sugar and saccharides analyses were performed on the same water
127 extract by an HPLC method using PAD (Pulsed Amperometric Detection) (model Dionex DX500 + ED40) with
128 Metrosep columns (Carb 1-Guard+A Supp15-150+Carb1-150) in the period before the year 2017. From 2017 to
129 the present, the measurement with ICS 5000 with pulsed amperometric detection (HPLC-PAD) was performed
130 following the CEN method (European committee for standardization, 2024). The analysis is isocratic with 15%
131 eluent of sodium hydroxide (200 mM), sodium acetate (4 mM), and 85% water at 1 mL min⁻¹.

132 The daily and weekly metals were measured by Inductively coupled plasma mass spectroscopy (ICP-MS) (ELAN
133 6100 DRC II PerkinElmer or NEXION PerkinElmer). The measurement was performed on the mineralization of
134 a 38 mm diameter punch of each filter, using 5 mL of HNO₃ (70 %) and 1.25 mL of H₂O₂ for 30 min at 180°C in
135 a microwave.

136 **2.2.2. OP analysis**

137 Two complementary OP assays, including the two probes ascorbic acid (AA) and dithiothreitol (DTT) were
138 performed on the same filters with PM₁₀ components analysis (from 02/01/2013 to 28/05/2023, n = 1570). Filter
139 samples are extracted using a simulated lung fluid which is the mixing of Gamble and DPPC
140 (dipalmitoylphosphatidylcholine) solutions, during 1h15 at 37°C, pH 7.4 , creating a physiological environment
141 for the extraction (Calas et al., 2017) . The AA method quantifies the consumption of ascorbic acid, an endogenous

142 antioxidant in the lung, by PM and was described in Calas et al. (2017, 2018). The reaction mixture (extract + AA)
143 was transferred to UV-transparent 96-well plates (CELLSTAR, Greiner-Bio), and the residual AA was measured
144 at 265 nm with a TECAN Infinite M200 Pro spectrophotometer. The AA consumption rate (nmol min⁻¹) reflects
145 the capacity of PM₁₀ to catalyze electron transfer from AA to molecular oxygen.

146 DTT assay relies on dithiothreitol, a chemical surrogate for cellular reducing agents, allowing for emulation of in
147 vivo interaction among PM₁₀ and biological reducing agents (for example, nicotinamide adenine dinucleotide
148 (NADH), nicotinamide adenine dinucleotide phosphate oxidase (NADPH)). After incubation of the PM
149 suspension within the lining fluid with DTT, the remaining DTT was titrated with 5,5'-dithiobis-(2-nitrobenzoic
150 acid) (DTNB) to form 5-mercaptop-2-nitrobenzoic acid (TNB). Absorbance at 412 nm (TECAN Infinite M200 Pro)
151 in 96-well plates provided the concentration of unconsumed DTT, from which the DTT consumption rate
152 (nmol min⁻¹) was calculated. The batches were standardized using a common control (lab's rooftop filter analysis
153 for every batch) to ensure consistency between batches.

154 After analysis, the OP activities were blank subtracted and then normalized using the PM₁₀ mass concentration
155 and the sampling air volumes. The mass-normalized OP (OP^m, nmol min⁻¹ µg⁻¹) represents the intrinsic OP of 1 µg
156 PM, while the volume-normalized OP (OP^v, nmol min⁻¹ m⁻³) represents PM-derived OP per m³ of air. Each sample
157 is analyzed in triplicate for AA and triplicate for DTT, respectively. Consequently, the OP values presented in the
158 study are the mean and the standard deviation of these replicates.

159 **2.2.3. Vertical temperature and other ancillary measurements**

160 Vertical temperature and humidity were measured every 30 minutes from November 2017 to May 2023 using
161 Tinytag TGP-4500 from Gemini Data Loggers. A Stevenson Type Screen protects each Tinytag loggers from
162 radiant heat (direct sunlight). Sensors are installed at a minimum of 3m from the ground. The measurements have
163 been performed at different elevations of the Bastille hill, located a few hundred meters from the city center
164 (5°43'37.0"E, 45°11'40.8"N), including z = 230, 309, 496, 916m altitudes.

165 Further, measurement of the PM₁₀ mass was conducted (hourly) using tapered element oscillating microbalances
166 equipped with filter dynamics measurement systems (TEOM-FDMS) at the same site as the filter collection. The
167 PM concentration used in this study is the 24-hour average concentration, which is associated with the days of
168 filter-based sample measurement (from 02/01/2013 to 28/05/2023).

169 **2.3. Multivariate imputation by chained equations (MICE)**

171 The daily concentration of metals was only accessed in some periods, with the number of samples being 362 of
172 the total of 1570 samples, which would severely limit the size of the inputs for the PMF processing. We used the
173 weekly concentration measured over the whole period to estimate the missing daily data using an imputation
174 method. The daily concentration of metals was imputed by using the MICE algorithm implemented with
175 multilinear regression (Azur et al., 2011). These values were modeled conditionally depending on the observed
176 values of the daily PM₁₀ and PM₁₀ components concentration (i.e., weekly concentration, PM₁₀, and PM₁₀
177 components concentration). These components are OC, EC, MSA, Levoglucosan, Mannosan, Polyols, NO₃⁻, SO₄²⁻
178 , Na⁺, NH₄⁺, K⁺, Mg²⁺, Cl⁻, Ca²⁺. The data preparation and imputation processes are implemented through 4 main
179 steps, as presented in S1 and Figure S1, Supplement. The validation of this imputation is shown in Table S1 and
180 Figure S2.

181 **2.4. Persistent inversions detection**

182 Thermal inversion occurs when the vertical temperature gradient between the ground-based and higher-altitude
183 stations is positive. However, this constraint is restrictive and limits thermal inversion detection, especially when
184 the calculation is on average daily temperature (Largeron and Staquet, 2016). Hence, the persistent inversion is
185 detected, as discussed in Largeron and Staquet (2016), for days with :

186
$$\text{average} \left(\frac{T_{916} - T_{230}}{\Delta z} \right)_{\text{Daily}} > \text{Mean} \left(\frac{T_{916} - T_{230}}{\Delta z} \right)_{\text{Winter}} \quad (1)$$

187 for more than 72 consecutive hours

188 with:

189 $T_{916} - T_{230}$ is the difference between temperature at ground-base station ($z = 230$ m altitude) and at high-elevation
190 station ($z = 916$ m);

191 Δz is the difference between the height of high and low elevations;

192 $\frac{T_{916} - T_{230}}{\Delta z}$: is the bulk temperature gradient between $z = 230$ and $z = 916$ m;

193 $\text{Mean} \left(\frac{T_{916} - T_{230}}{\Delta z} \right)_{\text{Winter}}$: is the mean bulk temperature gradient in wintertime (from November to March).

194 **2.5. Positive Matrix Factorisation (PMF)**

195 **2.5.1. PMF input**

196 EPA PMF 5.0 (Gary Norris et al., 2014) was used to identify and quantify the PM_{10} sources based on the observed
197 concentrations and their related uncertainties. The concept of PMF is to use the weighted least square fit method
198 and apply a non-negative constraint with the weight calculated based on analysis uncertainties (Paatero and
199 Tappert, 1994) (Eq. (S1), Supplement S2). In this study, the input matrix of the PMF comprises 25 chemical
200 species, including PM_{10} (set as the total variable), carbonaceous fractions (OC*, EC), ions (Cl^- , NO_3^- , SO_4^{2-} , Na^+ ,
201 NH_4^+ , K^+ , Mg^{2+} , Ca^{2+}), organic tracers (MSA, levoglucosan, mannosan, polyols) and trace metals (As, Ba, Cd,
202 Cr, Cu, Ni, Pb, Sb, V, Zn). The trace metals were the daily measured metals in some periods (2013, 2017-2018,
203 2020-2021) and the daily imputed metals. The OC* (=OC minus the sum of the carbon mass from the organic
204 tracers used in the input variables) was used to avoid considering twice the mass of C atoms in organic markers.
205 Polyols were calculated as the sum of arabitol and mannitol, supposing that their origin is similar (Samaké et al.,
206 2019a). The input uncertainties were calculated based on the concentrations and the uncertainties in the analysis
207 (Gianini et al., 2012; Waked et al., 2014). Details on the calculation of OC* and uncertainties of PMF input are
208 presented in Section S3, Supplement. The selection of the input variables is guided by our previous yearly PMF
209 studies at this site (Borlaza et al., 2021; Srivastava et al., 2018; Weber et al., 2019).

210 **2.5.2. Set of constraints**

211 The application of PMF constraints is recommended in the European guide on air pollution source apportionment
212 with receptor models (Belis et al., 2014) to avoid mixing between some factors and reduce the uncertainty of the
213 rotational ambiguity. The constraints used in this study are also based on the previous PMF studies in Grenoble
214 (Borlaza et al., 2021; Srivastava et al., 2018; Weber et al., 2019) and are detailed in Table S3.

215 **2.5.3. Choice of the final PMF solution**

216 Several solutions, including those from 4 to 11 factors, were investigated to determine the optimal output. This
217 selection is based on the ratio of $Q_{\text{true}} / Q_{\text{robust}}$ (evaluating the outlier's effect), the clarity of the chemical profile,
218 the contribution of factors to PM_{10} , the correlation between measured and predicted concentration, and the stability
219 of the solution. This stability was evaluated using the bootstrapping (BS) and displacement (DISP) methods. BS
220 analysis randomly resamples the data observation matrix and uses it to run a new PMF. The base-run and boot-
221 run factors are matched if their correlation exceeds the threshold (generally chosen at 0.6). DISP estimates each
222 species' uncertainty in the factor profile by fitting the model many times until this variable turns displaced (upper
223 or lower) from its fitted value. The details of the set criteria for validation are presented in S4.

224 To evaluate the stability of the PMF solution over time (including possible changes in the chemical profiles of the
225 sources), we also implemented separated PMF SA for every successive period of 3 years (2013-2016, 2017-2020,
226 2021-2023) and then we investigated the homogeneity of the chemical profiles by using the Pearson distance (PD)
227 and standardized identity distance (SID) metrics (Belis et al., 2015). The chemical profiles of PMF solutions every
228 3 years and 11 years, and those published in Borlaza et al. (2021) are compared to assess the homogeneity of the
229 chemical profiles.

230 **2.6. Regression techniques for PM_{10} OP SA**

231 The regression technique is applied to apportion OP^v (AA, DTT) and PMF-derived PM_{10} sources' contribution, as
232 expressed in Eq.2. Principally, OP^v ($\text{nmol min}^{-1} \text{m}^{-3}$) is treated as a dependent variable, and PMF-derived PM_{10}
233 sources' contribution ($\mu\text{g m}^{-3}$) are independent variables. The OP SA methodology in this study follows the
234 methodology reported by Ngoc Thuy et al. (2024).

$$235 \quad OP_v = \sum_p^{i=1} OP_m^i * PM^i + e \quad (2)$$

236 Where:

237 OP_v is the volume-normalized OP ($\text{nmol min}^{-1} \text{m}^{-3}$)

238 p is the number of PMF-derived PM_{10} sources

239 OP_m^i is the regression slope, denoted as the intrinsic OP of source i ($\text{nmol min}^{-1} \mu\text{g}^{-1}$)

240 PM^i is the contribution of source i to PM_{10} ($\mu\text{g m}^{-3}$)

241 e is the residual of the regression technique ($\text{nmol min}^{-1} \text{m}^{-3}$)

242 The appropriate regression tool is selected based on the collinearity among independent variables and the variance
243 of regression residuals (Ngoc Thuy et al., 2024). The collinearity among PMF-derived sources was tested using
244 the variance inflation factor (VIF), which is calculated using Eq. (S3) in Supplement S2 (Craney and Surles, 2002;
245 O'Brien, 2007; Rosenblad, 2011). The variance of the regression residual is assessed using the Goldfeld-Quandt
246 test (Goldfeld and Quandt, 1965) to investigate if the regression residual varies by the value of the dependent
247 variable (OP^v). The most appropriate regression method is selected among a wide choice of possible tools
248 (including ordinary least square, weighted least square, positive least square, Ridge, Lasso, random forest, and
249 multiple layer perceptron), following the methodology developed by Ngoc Thuy et al. (2024). It is performed with
250 considering the characteristics of the data and comparing the accuracy metrics (R-square, root mean square error,
251 and mean absolute error) for each of them. For instance, if the regression residual is constant (homoscedasticity),

252 the model ordinary least square (OLS) and Positive least square (PLS) are satisfactory. On the other hand, if the
253 regression residual varied with the dependent variable (heteroscedasticity), the models incorporating some sort of
254 weighting are chosen (including weighted least squares (WLS) and weighted positive least squares (wPLS)),
255 where the weighting is the standard deviation of replicated OP analyses.

256 The most appropriate model was trained by randomly choosing 80% of the dataset and validated with the
257 remaining 20%. The model was run 500 times to ensure the robustness of the results, especially considering the
258 remarkable seasonality of many components in the dataset. The contribution to OP of each source is calculated
259 by multiplying its contribution to PM_{10} with the arithmetic mean intrinsic OP (or regression slope) of the 500
260 iterations.

261 **2.7. Seasonal-trend using LOESS decomposition**

262 Seasonal-trend decomposition using LOESS (SLT) was developed by RB Cleveland et al. (1990) and is a robust
263 method for decomposing time series into trends, seasonality, and residuals. This method uses LOESS, a method
264 for estimating the non-linear relationships to decompose a time series. In our case, we used monthly average
265 concentration as input data in order to have a more robust data set, smoothing high variability noise. The trend
266 component is first calculated by applying a convolution filter to the data. Then, this trend is removed from the
267 series. Finally, the average of this detrended in each period is the seasonal component. The residuals can be
268 explained neither by trend nor by season. The STL is an iterative model that uses LOESS to smooth seasonal and
269 trend components to obtain the minimum residuals. Further, in STL decomposition, the outliers in the data are
270 given less weight in the estimation of trend and season. The STL model is described in the equation below:

$$271 \quad y_t = S_t + T_t + R_t \quad (t = 1, 2, \dots, n) \quad (3)$$

272 where, in our case, y_t is the monthly contribution of PMF-derived sources, S_t is the seasonal component, T_t is the
273 trend component, and R_t denotes the residual component. The seasonal frequency was chosen 6 months before
274 and 6 months after the evaluated month (seasonal frequency = 13 months) to estimate the yearly trend cycle.
275 Hence, the first and last 6 months of the decomposition time series were removed from the results to prevent edge
276 effects.

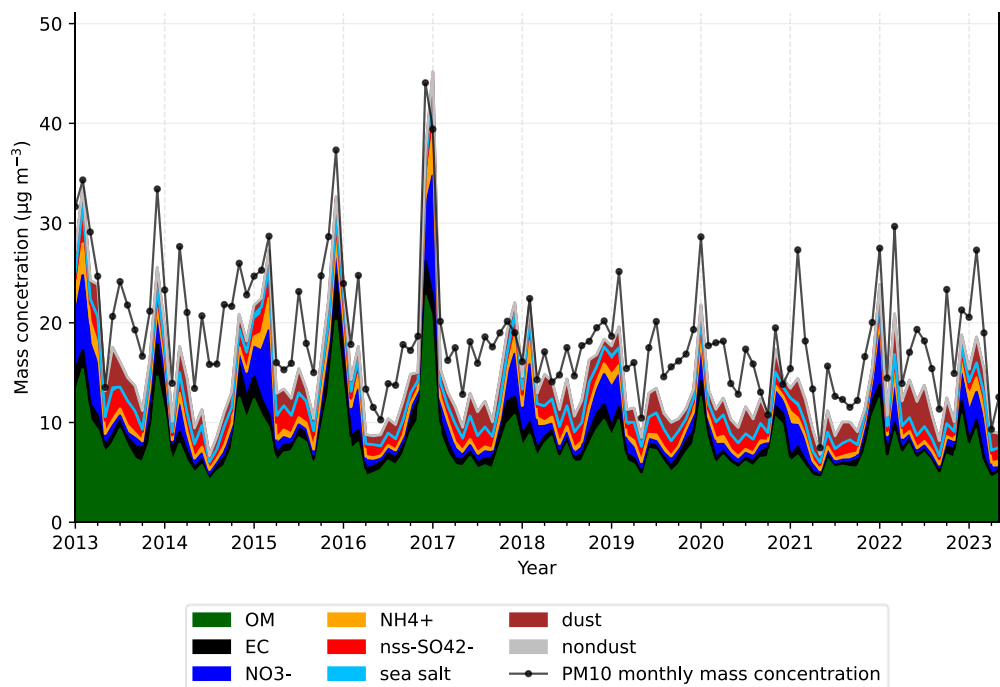
277 The long-term trend of PM_{10} sources was accessed by applying the STL model to the monthly contribution of
278 sources to PM_{10} (output of PMF). The fit line of the trend was assessed by using ordinary least squares linear
279 (OLS). The annual rate change of the trend is the slope of the fit line multiplied by 12 months ($\mu\text{g m}^{-3} \text{yr}^{-1} / \text{nmol}$
280 $\text{min}^{-1} \mu\text{g}^{-1} \text{yr}^{-1}$). The STL decomposition and the fit line of the trend were performed in Python 3.9 using the
281 package "statsmodels" (Seabold and Perktold, 2010).

282 **3. Results and discussion**

283 **3.1. Evolution of PM_{10} concentration and chemical components**

284 The annual average concentration of PM_{10} , considering all available daily measurements, is $19.0 \pm 10.6 \mu\text{g m}^{-3}$ for
285 the whole studied period (2013-2023). The highest annual concentration is observed in 2013 ($24.4 \pm 13.7 \mu\text{g m}^{-3}$),
286 and the lowest is in 2021 ($15.3 \pm 9.8 \mu\text{g m}^{-3}$). The number of days with concentrations surpassing the European
287 standard daily thresholds ($40 \mu\text{g m}^{-3}$) is 176 days in 11 years, representing 4.6% of the total observed days, which
288 are principally found in the cold season (Nov, Dec, Jan, Feb, Mar).

289 The PM₁₀ main components are organic matter (assuming OM = 1.8*OC (Favez et al., 2010)), representing on
 290 average over the overall period 41.3±8.0% of PM₁₀ mass concentration, followed by dust (9.6± 4.4%), nitrate
 291 (NO₃⁻, 7.5±6.2%), non-sea salt sulfate (nss-SO₄²⁻, 7.4±2.4 %), elemental carbon (EC, 5.5±2.5%), ammonium
 292 (NH₄⁺, 3.9±2.0%), sea salt (Na⁺ and Cl⁻, 1.7±0.8%) and other non-dust elements (Cu, Pb, V, Zn, representing
 293 0.2±0.1%). These main composition fractions are estimated using the formula as shown in S2, Eq. (S4). The
 294 monthly evolutions of PM₁₀ and its main chemical components for the whole period are shown in Figure 2. The
 295 maximum concentration of PM₁₀ was observed in winter months (December, January, and February),
 296 corresponding to the highest concentration of OM and EC (7.82±3.11 $\mu\text{g m}^{-3}$ and 1.09±0.74 $\mu\text{g m}^{-3}$, respectively).
 297 Nitrate concentrations are higher in the middle of winter and the early spring, corresponding also with the high
 298 concentrations of ammonium (1.63±1.87 and 0.78±0.62 $\mu\text{g m}^{-3}$). The agricultural activities (especially manure
 299 spreading) could explain this high contribution in spring under humidity and temperature conditions favoring the
 300 condensation of ammonium nitrate in the particulate phase. Nss-sulfate concentrations are more abundant in the
 301 warmer season (summer), where the photochemical production is favorable. No clear seasonal pattern could be
 302 observed for other components (sea salt, dust, non-dust, estimated as described in section S2), suggesting that the
 303 emissions of these components are stable for the whole year. At first glance, decreasing trends appear visible for
 304 PM₁₀ and OM, EC, NO₃⁻, NH₄⁺, and non-dust components, while sea salt, dust, and nss-SO₄²⁻ do not seem to
 305 present significant trends. With chemical components coming from several emission sources, an advanced
 306 analysis, including a PMF model followed by an STL decomposition, was performed to assess the trend of PM₁₀
 307 sources. The result of the PMF model is presented in section 3.2, and the tendencies of PM₁₀ sources and OP are
 308 shown in sections 3.3 and 3.4, respectively.



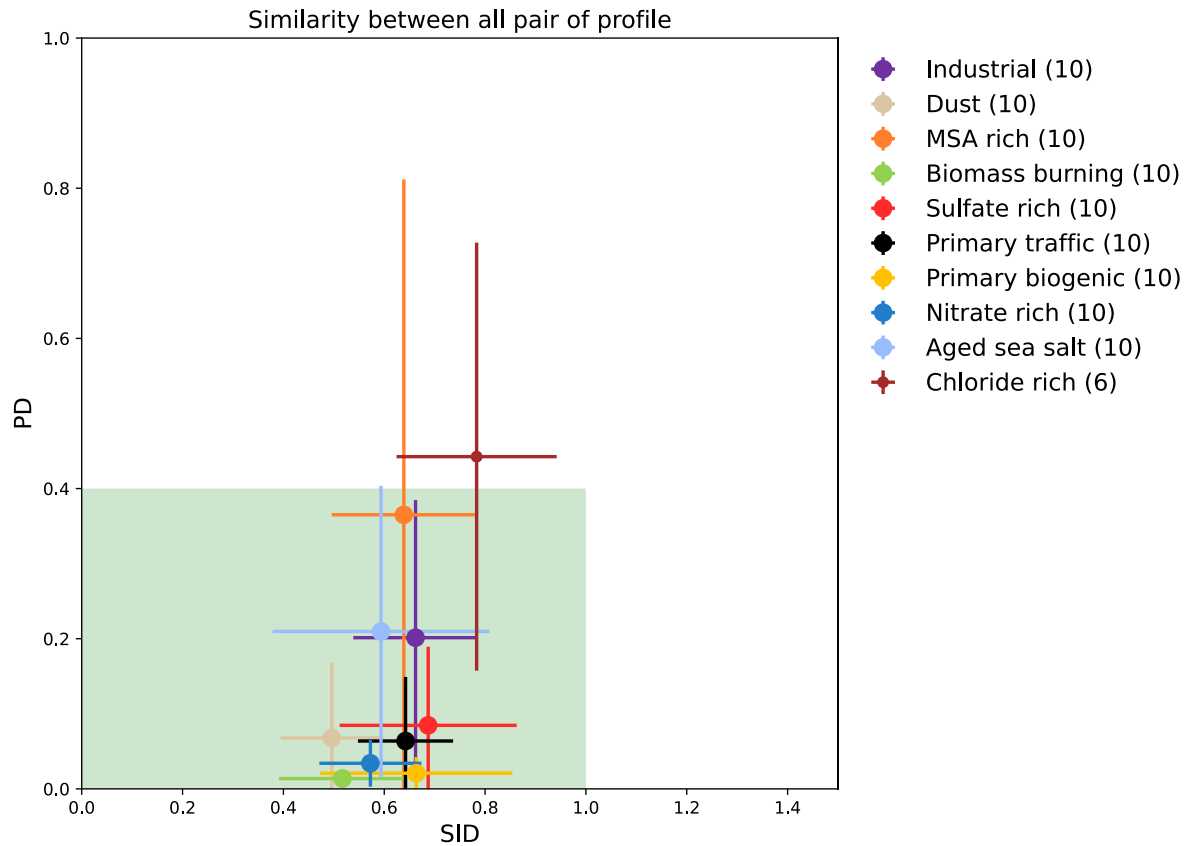
309
 310 **Figure 2. The average monthly evolution of PM₁₀ and its main components from 2013 to 2023. The line represents the**
 311 **monthly average concentration of PM₁₀ measured by TEOM-FDMS.**

312 **3.2. PM₁₀ sources apportionment**

313 **3.2.1. PMF chemical profiles**

314 Using a unique chemical profile for each of the sources for such a long-term period can potentially limit the
315 assessment of its evolution (Borlaza et al., 2022a). To evaluate such a phenomenon in our case, we investigated
316 the chemical profile and contribution of PM₁₀ sources for three distinct periods (2013-2016, 2017-2020, 2021-
317 2023) and compared the results with those for the full 11-year period, as well as to the results presented in (Borlaza
318 et al. (2021) for the year 2017. Particularly, we checked the similarity of the chemical profiles of these PMF
319 solutions using PD and SID metrics (Belis et al., 2015).

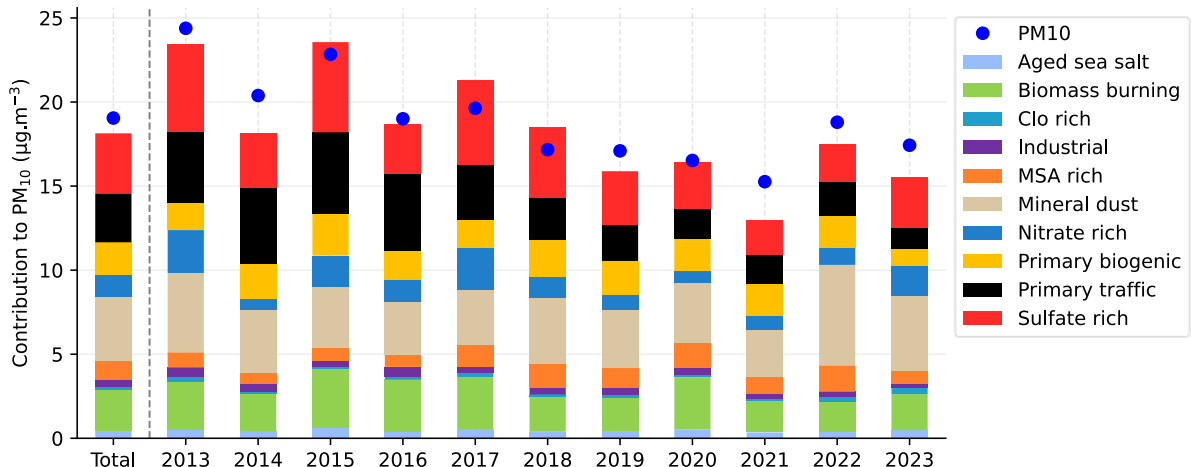
320 For each SA, the PMF solution was tested from 4 to 11 factors and validated by the criteria presented in section
321 S4. The results of these validations (Q_{true}/Q_{robust} , bootstrap run, displacement run, and statistical validation) are
322 presented in S5, Tables S4, S5 and S6. The runs of 4 to 9 factors returned at least one merging factor, and the
323 solution with 11 factors led to a factor without geochemical identity. Finally, for each PMF tested (11 years, 2013-
324 2016, 2017-2021, 2022-2023), the best solution includes 10 PM₁₀ sources, with mineral dust, sulfate-rich, primary
325 traffic, biomass burning, primary biogenic, nitrate-rich, MSA-rich, aged sea salt, industrial, and chloride-rich.
326 The similarity of the chemical profiles is presented in Figure 3. Most of the factors (i.e., aged sea salt, mineral
327 dust, primary biogenic, biomass burning, primary traffic, industrial, nitrate-rich, and sulfate-rich) present quite
328 homogenous chemical profiles over the 3 successive periods, indicating that these source profiles are quite stable
329 during the full 11-year period and similar compared to sources reported in Borlaza et al. (2021). The MSA-rich
330 and chloride-rich sources are the most divergent but are still within the limit of the accepted PD and SID range;
331 however, their standard deviations for PD are slightly higher than for the other sources (Figure 3). This is due to
332 differences in the contributions of SO₄²⁻ in the chemical profile of MSA-rich, which varied from 6 % to 17%, and
333 that of Cl⁻ (73% - 83%) in the chloride-rich factor. In a previous study, Weber et al. (2019) also reported that the
334 proportion of SO₄²⁻ in the MSA-rich source can significantly vary across French sites, from 6% to 24%. The
335 chloride-rich source in our study (previously named sea/road salt in Borlaza et al. (2021) is essentially composed
336 of a high proportion of Cl⁻, with less than 10% of Na⁺ and some metals (Cu, Mn, Ni, V). This source is detected
337 in other alpine valley environments (Glojek et al., 2024), with a similar temporal evolution as here. Since chloride
338 depletion from the particulate phase can greatly depend on solar radiation, relative humidity, and temperature, the
339 chemical profile of this factor can vary on different time scales. This source was also observed to be heterogeneous
340 in the three neighboring sites investigated within 15 km in the previous study in Grenoble (Borlaza et al., 2021).
341 Nevertheless, it should be noted that it represents only a very minor fraction of the PM₁₀ total mass (about 1%).
342 With these stabilities of the chemical profiles over the years, the solution for the 11-year SA is considered suitable
343 for further data analyses in this paper. In the next section (3.3.2), we investigate how the contribution of these
344 sources to total PM₁₀ loadings changed over time.



345
346 **Figure 3.** Similarity plots of the chemical profiles of the solution for the 11-year SA against the 3 SA solutions every 3
347 years, and those presented by Borlaza et al. (2021). The shaded area (in green) shows the limit of the homogeneous
348 chemical profile. For each point, the error bars represent the standard deviation when comparing all pairs of SA
349 solutions (number of pairs in parentheses in the legend).

350 3.2.2. Variations of the source's contribution in the 11-year PMF SA

351 As presented in Figure 4, the optimal PMF solution for the 11-year time series identifies 10 PM₁₀ sources, with
352 the contributions of mineral dust (20.9%), sulfate-rich (19.7%), traffic (16.0%), biomass burning (13.5%), primary
353 biogenic (10.7%), nitrate-rich (7.2%), MSA-rich (6.2%), industrial (2.2%), aged sea salt (2.5 %), and chloride-
354 rich (1.0%). The chemical profile and contribution of each source are shown in Figures S3 and S4, respectively.
355 Even though the chemical profiles are homogenous, the contributions of these sources show minor differences
356 from those reported for this same site by Borlaza et al. (2021) and Srivastava et al. (2018), partly because of the
357 differences in the respective periods of the studies. However, the main sources are similar, i.e., SIA (nitrate and
358 sulfate-rich), mineral dust, biomass burning, and primary traffic. Similar general results are also presented for
359 Swiss Alpine (Ducret-stich and Tsai, 2013), French Alpine (Weber et al., 2018), and Slovenian Alpine areas
360 (Glojek et al., 2024), showing biomass burning and secondary inorganic aerosols being the most abundant
361 contributions to PM mass. Primary biogenic and MSA-rich sources are the biogenic sources rarely reported in the
362 literature; however, they account together for 17% of total PM₁₀ mass on average in our study, which is in line
363 with those reported in urban background sites in France (Samaké et al., 2019b; Weber et al., 2019). The absolute
364 PM₁₀ source contributions are also compared to the average annual concentration of PM₁₀ mass to demonstrate
365 the ability of the PMF model to reconstruct the PM₁₀ mass. The difference between observed and reconstructed
366 PM₁₀ concentrations on the 11-year average is about 1 $\mu\text{g m}^{-3}$ (5 %), with no more than 2 $\mu\text{g m}^{-3}$ for any single
367 year, demonstrating that the PMF model performs well at reconstructing the PM₁₀ concentrations.



368
369 **Figure 4. The absolute average contribution of sources to PM₁₀ for every year and the 11 years (total), and the**
370 **concentration of PM₁₀ (blue circle).**

371 Significant trends in source contributions over this 11-year period are detected (and discussed in section 3.3);
372 nevertheless, the main contributors to the total PM₁₀ mass do not change, with mineral dust, biomass burning,
373 sulphate-rich, nitrate-rich, and primary traffic being the main contributors to PM₁₀. The highest PM₁₀
374 concentrations (observed in winter/spring 2013 and 2015) are associated with the highest contribution of SIA and
375 biomass burning sources. On the other hand, the relative contribution of SIA and biomass burning showed a
376 negligible difference (varied from 0.3 to 4%) between these years compared to 2014 and 2016 (Figure S5). The
377 lowest PM₁₀ annual concentration was detected in 2021, notably when the third COVID-19 pandemic lockdown
378 restrictions applied in France. In addition, the relative contributions (see Figure S5) showed only small changes
379 compared to those in other years, with an increasing contribution of primary biogenic sources in 2021 (4%
380 compared to 2020), and only a very light decrease in the anthropogenic sources.

381 The decrease in PM₁₀ annual average concentrations observed since 2017 is associated with decreases in the
382 contribution of some of the anthropogenic PM₁₀ sources. However, using yearly averages for trend analysis may
383 prevent a proper understanding of the variation in time and of the estimation of the trends based on monthly
384 averages, which might be more informative, as discussed in section 3.3.

385 3.3. Trends in sources' contributions

386 3.3.1. Mean rate change in the contribution of PM₁₀ sources

387 The source contribution trend analysis was achieved through STL deconvolution (see section 2.6). These trends
388 for all sources over the full period of the study are presented in Table 1. In this table, the part labeled 'Rest'
389 represents the difference between the total PM₁₀ measured mass and the sum of the mass of all PMF-derived
390 factors in order to assess any trend of the unresolved part of PM₁₀ within our SA study.

391 PM₁₀ concentrations present a downward trend from 2013 to 2023, with an average diminution of 0.73 µg m⁻³ yr⁻¹ (3.9%) (S6, Figure S6). Such a downward trend of PM₁₀ in Grenoble is in line with that observed in other urban
392 sites in Europe (Aas et al., 2024; Borlaza et al., 2022a; Caporale et al., 2021; Colette et al., 2021; Gama et al.,
393 2018; Li et al., 2018; Pandolfi et al., 2016).

395 The reduction of PM₁₀ in Grenoble during this period is significantly larger than that in 30 rural sites of the
396 European Monitoring and Evaluation Programme (EMEP) from 2000 to 2017, which show reductions of PM₁₀

397 from -1.5% to -2.5% (-0.008 to -0.58 $\mu\text{g m}^{-3}$) (Colette et al., 2021). However, the results of our study are highly
398 coherent with results from Aas et al. (2024), presenting a reduction of PM_{10} in 2 rural sites in France (La Tardi  re
399 and Revin) of $-3.5\% \text{ yr}^{-1}$ between 2005 and 2019. The reduction of PM in this Grenoble site, as an urban site,
400 being higher than those at the rural sites, is due to the changes in specific emission activities at the site. While in
401 the rural sites, the PM emission are influenced by long range transport activities, the PM at the urban site is usually
402 largely impacted by different local activities (Borlaza et al., 2022b). Further, France is amongst the EU countries
403 with the highest reduction trend, as presented by Aas et al. (2024).

404 The anthropogenic sources, such as primary traffic, sulfate-rich, and biomass burning, display the highest decrease
405 between 2013 and 2023 in Grenoble, with a reduction of 12.9, 6.9, and 5.5% (0.37, 0.25, and 0.13 $\mu\text{g m}^{-3} \text{ yr}^{-1}$),
406 respectively. The other anthropogenic sources also present significant decreasing trends; however, these trends
407 are much lower (nitrate-rich: $-0.11 \mu\text{g m}^{-3} \text{ yr}^{-1}$, industrial: $-0.02 \mu\text{g m}^{-3} \text{ yr}^{-1}$). The downward trends of these
408 anthropogenic sources (mainly traffic, SIA, and industrial) were also underlined for other European urban sites
409 (Colette et al., 2021; Diapouli et al., 2017; Pandolfi et al., 2016) with various approaches. For instance, a similar
410 approach using PMF (albeit without organic markers) was followed by Pandolfi et al. (2016), investigating the
411 Mann-Kendall trend of PMF-derived sources, and reported an almost equivalent downward trend of the sulfate-
412 rich factor of 53% (i.e., $0.53\% \text{ yr}^{-1}$) between 2004 and 2014 in Spain. The decreasing trends of primary traffic,
413 domestic biomass burning, and industrial emissions are potentially influenced by the reduction in primary
414 emissions due to various abatement strategies (as discussed in the following subsections, notably in 3.3.3 and
415 3.3.4).

416 Conversely, natural sources such as mineral dust and chloride-rich factors do not show any significant trend or
417 follow a very weak one (aged sea salt, primary biogenic). MSA-rich is the only source that displays a significant
418 upward trend, with an increase of $0.08 \mu\text{g m}^{-3} \text{ yr}^{-1}$; further studies would be needed to relate this last increase to
419 changes in precursor emissions or reactivity during transport. Finally, the low evolutions in the contributions of
420 the natural sources demonstrate that the reduction in PM_{10} in Grenoble is essentially related to the reduction of
421 anthropogenic activities, especially sources related to traffic and domestic biomass burning activities.

422
423 **Table 1. Trend of PM_{10} sources and PM_{10} (in $\mu\text{g m}^{-3} \text{ yr}^{-1}$ and $\% \text{ yr}^{-1}$).**

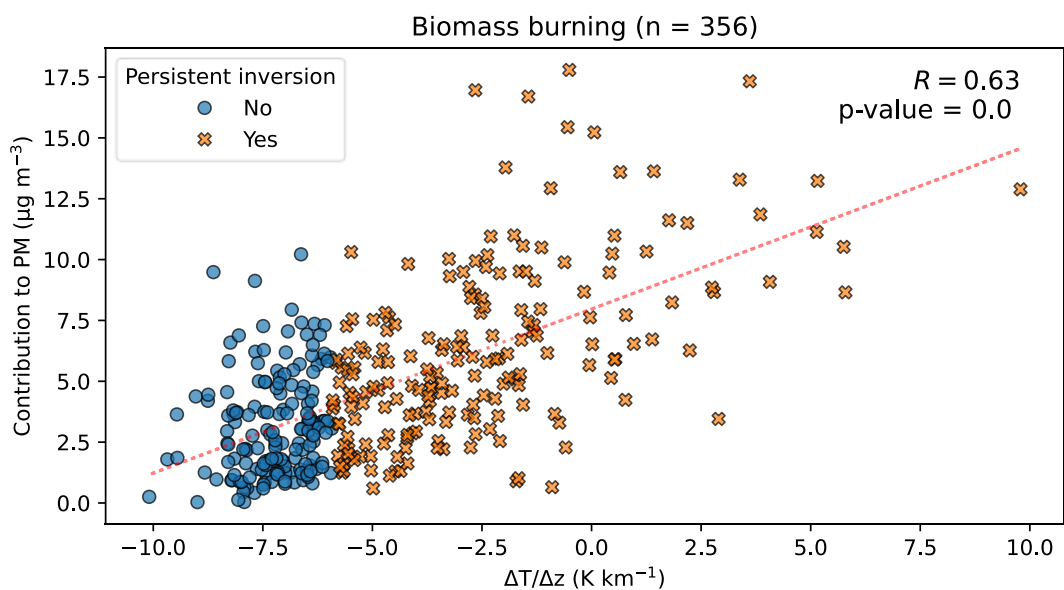
	Absolute trend ($\mu\text{g m}^{-3} \text{ yr}^{-1}$)	Relative trend ($\% \text{ yr}^{-1}$)	P-values	R^2
Aged sea salt	-0.01	-2.50	<<0.01	0.22
Biomass burning	-0.13	-5.48	<<0.01	0.98
Chloride rich	0.00	1.18	0.01	0.07
Industrial	-0.02	-5.36	<<0.01	0.40
MSA rich	0.08	6.63	<<0.01	0.64
Mineral dust	0.04	1.03	0.02	0.05
Nitrate rich	-0.11	-8.08	<<0.01	0.94
Primary biogenic	-0.01	-0.49	0.03	0.04
Primary traffic	-0.37	-12.85	<<0.01	0.94
Sulfate rich	-0.25	-6.89	<<0.01	0.70
PM_{10}	-0.73	-3.89	<<0.01	0.68
Rest	-0.11	-2.13	<<0.01	0.39

425 **3.3.2. Potential influence of meteorology**

426 The STL deconvolution is inherently constructed to separate the yearly and seasonal variations from the long-
 427 term trends. While we discuss the long-term trends of the sources in other sections (3.3.1, 3.3.3, and 3.3.4), it is
 428 also interesting to evaluate the impact of the meteorology on the seasonal variations of the concentrations. It is
 429 well known that inversion layers in the lower atmosphere are extremely important for the modulation of the
 430 concentrations at the ground, particularly in the context of Alpine valleys during winter (Carbone et al., 2010;
 431 Glojek et al., 2022). In this section, we tried to better evaluate these impacts on the concentrations from the sources
 432 of PM in the case of our time series.

433 This was considered with the measurements of temperature along the slopes of the mountains very close to the
 434 city center (as described in section 2.2.3), for the winter periods of 2017-2023. It has been previously shown by
 435 Allard et al. (2019) that such measurements are representative of the temperature in the valley, despite the potential
 436 influence of wind slopes. We particularly considered the temperature gradient over the first 700 m above ground
 437 and the number of days with persistent inversion, as defined in section 2.2.3.

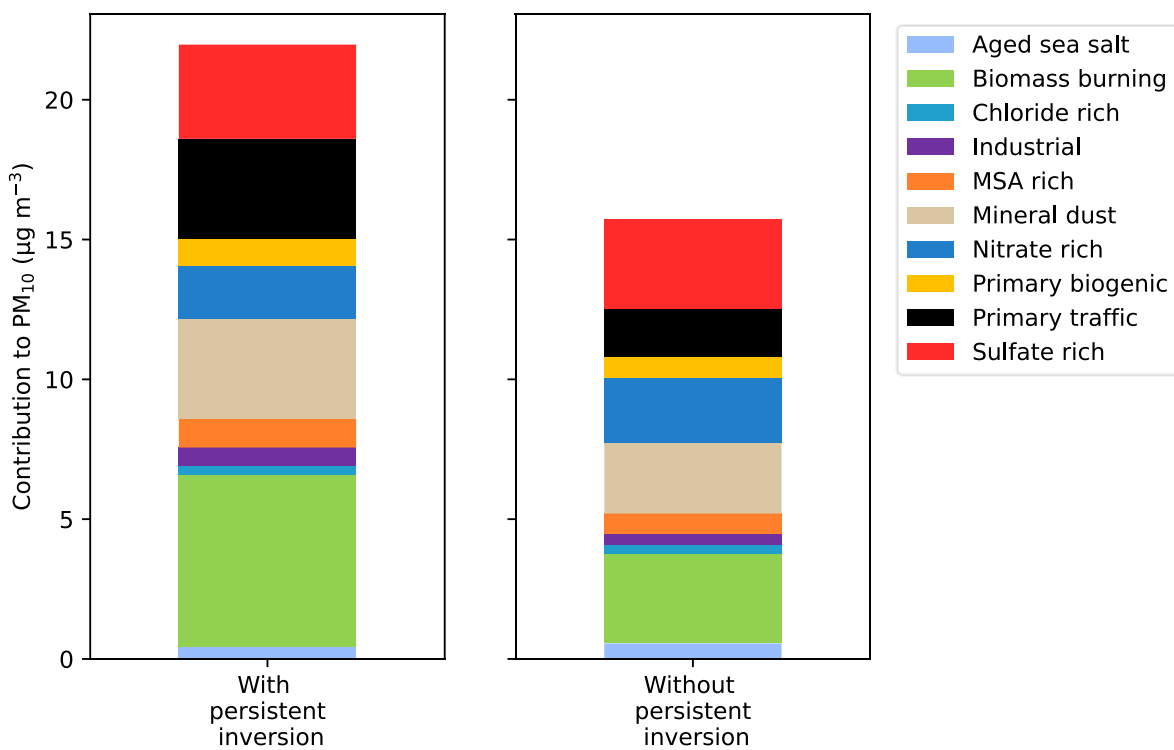
438 The analysis of the relationship between the PM_{10} and bulk temperature vertical gradients ($\Delta T/\Delta z$) in winter (Nov,
 439 Dec, Jan, Feb, Mar), summer (May, June, Jul, Aug), and transition season (remaining months) reveals that thermal
 440 inversion events and high PM_{10} concentration are mainly occurring in winter time (Supplement S7, Figure S8)
 441 during the 5 years of the study. Periods of persistent temperature inversion were assessed based on the condition
 442 in Eq. 1, which detected 79 persistent inversion days in series from 4 to 22 consecutive days, for the winter periods
 443 2017-2023. A meaningful correlation is obtained between PM_{10} concentrations and bulk temperature vertical
 444 gradient (r reaching 0.60, $p < 0.001$) for these winter months and even better when considering only the persistent
 445 inversion periods (r reaching 0.67, $p < 0.001$) for individual years (Table S7).



446
 447 **Figure 5.** Daily concentrations of biomass burning to PM_{10} and daily temperature gradients ($\Delta T/\Delta z$) during the
 448 winter periods (from November to March) of 2017-2023. The dotted red line is the linear regression fit. The blue
 449 circle symbols denote days when persistent inversion does not occur, and the orange multiple symbol denotes days
 450 when persistent inversion occurs.

451
 452 The distribution between the daily PM_{10} concentration and daily average $\Delta T/\Delta z$ in winter months revealed that
 453 the majority of PM_{10} concentration peaks (in excess of $40 \mu g m^{-3}$) occur during the persistent inversion days

454 (Figure S9). However, it also shows that a few high PM₁₀ concentrations could be found on the days without
 455 persistent inversion; meanwhile, the days with persistent inversion do not always have high PM₁₀ concentrations.
 456 This result is not surprising since the concentration of PM₁₀ is not only associated with thermal inversion events
 457 but also depends on other meteorological conditions (precipitation, heat deficit) and the variation of pollutant
 458 emissions (Carbone et al., 2010; Largeron and Staquet, 2016).
 459 Interestingly, the impact of persistent inversion days on PM₁₀ concentrations from the residential biomass burning
 460 source is larger than that for other sources or total PM₁₀ (Figure 5), with a higher correlation (0.63). In addition,
 461 the contribution of this source is systematically lower during non-inversion days, and large concentrations are
 462 essentially made during persistent days. The large impact of the inversions on the local sources is confirmed when
 463 comparing the source contribution of the inversion days vs non-inversion days (Figure 6). This figure shows both
 464 the large increase in average PM₁₀ concentrations and also the contributions of the local sources (emissions from
 465 residential biomass burning, traffic, industries, mineral dust probably from resuspension) in the cases of inversion
 466 days during winter. Conversely, long-range transport sources (sulfate-rich, nitrate-rich) tend to be less important
 467 during these inversion days. A similar pattern is observed for the relative contribution of sources to PM (Figure
 468 S.10), in which the significant contribution of biomass burning, dust, industrial, and primary traffic is detected
 469 during inversion events. The trends of the two most important local anthropogenic sources (domestic biomass
 470 burning and traffic) are further discussed in the next sections.

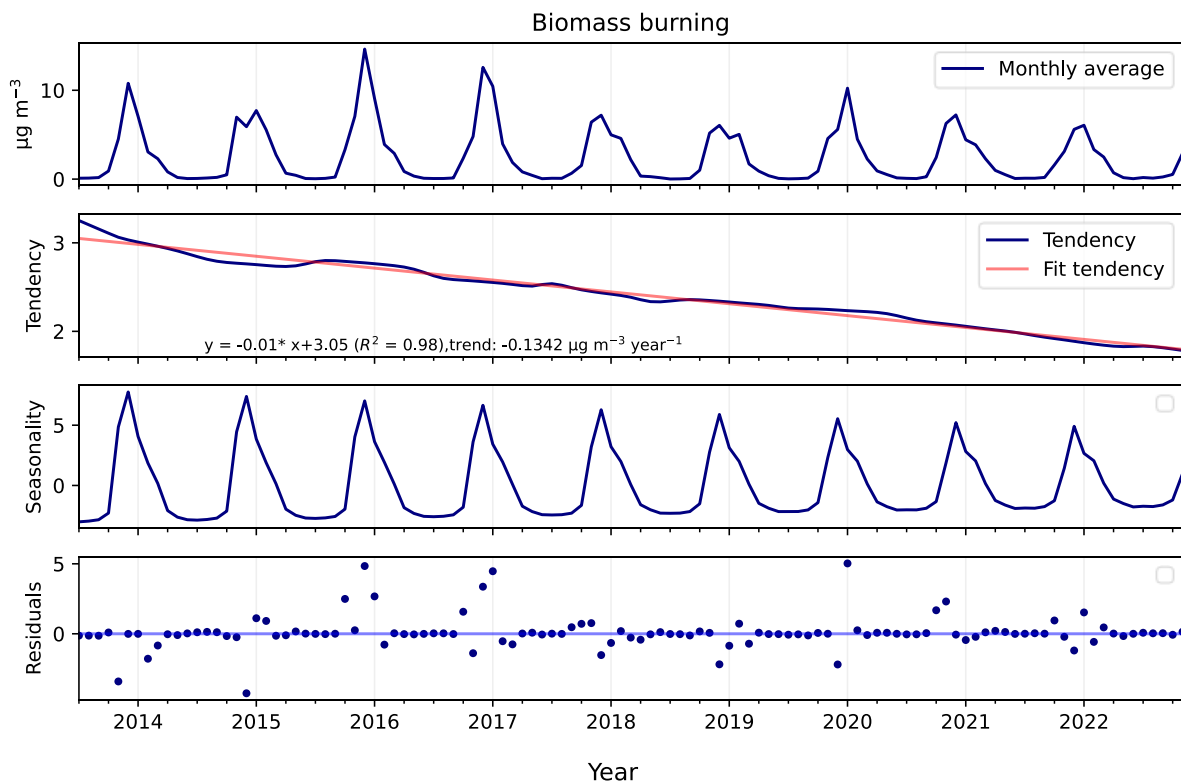


471
 472 **Figure 6. Contribution of the different sources to the PM₁₀ composition for days with persistent inversion vs non-**
 473 **inversion days of the winters 2017-2023.**

474 3.3.3. Trend in biomass burning contributions

475 The trend of the domestic biomass burning PM₁₀ concentrations is investigated via an STL decomposition analysis
 476 on this PMF-derived source (Figure 7), indicating a statistically significant decreasing trend from 2013 to 2023
 477 (p-values <<0.01). The seasonal estimate shows the highest values in the winter season (Nov, Dec, Jan), with a

478 visual trend to a smoothing of the peak concentrations; conversely, from Mar to Sept, the seasonal variations
 479 showed constantly lowest values. Extreme residual values were detected in the winter months of 2016, 2017, and
 480 2021, explained by high-concentration episodes of PM_{10} , where the concentration exceeded the European standard
 481 for PM_{10} concentration in 24 hours (PM_{10} concentration varied from 50 to $78 \mu\text{g m}^{-3}$). The linear fit line of the
 482 trend is highly significant with $R^2 = 0.97$, with a reduction of $134 \text{ ng m}^{-3} \text{ yr}^{-1}$ ($-5.5\% \text{ yr}^{-1}$).
 483

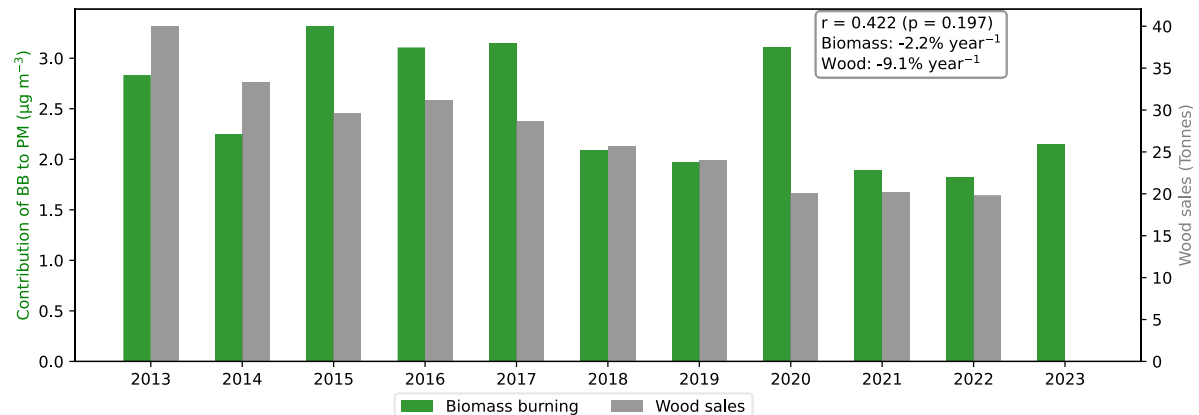


484
 485 **Figure 7. The season-trend (STL) decomposition of biomass burning**

486 This reduction of biomass burning concentrations in Grenoble is 4 times higher than the results from a long-term
 487 study (2012 to 2020) in a French rural site - (Observatoire Pérenne de l'Environnement, OPE) (Borlaza et al.,
 488 2022a) - estimated at $33 \text{ ng m}^{-3} \text{ yr}^{-1}$ over the same period. Besides the study of Borlaza et al. (2022a), there are
 489 no previous PMF studies describing any trend of biomass burning factors. Nevertheless, similar trends were found
 490 for concentrations of biomass burning tracers. In particular, Font et al. (2022) presented a downward trend of
 491 PM_{10} concentration from wood burning (a reduction from 1.5 to $3.8\% \text{ yr}^{-1}$) in urban sites in the United Kingdom
 492 from 2010 to 2021, by calculating the emission of wood burning from aethalometer measurement. Similarly, from
 493 2002 to 2018 in Norway, a downward trend of $2.8\% \text{ yr}^{-1}$ was also detected for levoglucosan (Yttri et al., 2021).
 494 Additionally, Colette et al. (2021) modeled the trend of the emissions from different activities in Europe, showing
 495 that the trend of PM_{10} heating emissions was decreasing in the period 2000-2017, with mean rate values varying
 496 from 0.8 to $3.3\% \text{ yr}^{-1}$ for 30 European countries (EMEP monitoring sites). Even though the chemicals and the
 497 period of these studies differ, a decreasing trend is generally observed among European cities, including the one
 498 investigated here. Interestingly, the biomass burning source in Grenoble shows the strongest decreasing trend,
 499 with a reduction of $5.5\% \text{ yr}^{-1}$.

500 Since the biomass burning sources in Grenoble are related to residential heating, the observed reduction of the
 501 concentrations from this source could be linked to household behaviors (including appliance renovation) on top

502 of the changes in meteorological conditions, lowering the overall heating demand. The average annual biomass
 503 burning sources PMF-derived is compared to the local PM_{10} emission inventory for residential heating (tonnes)
 504 in the Grenoble metropolis, estimated by the regional air quality monitoring agency (Atmo AuRA), to confirm
 505 the trend of biomass burning (Figure 8). This emission inventory has been available until 2022.

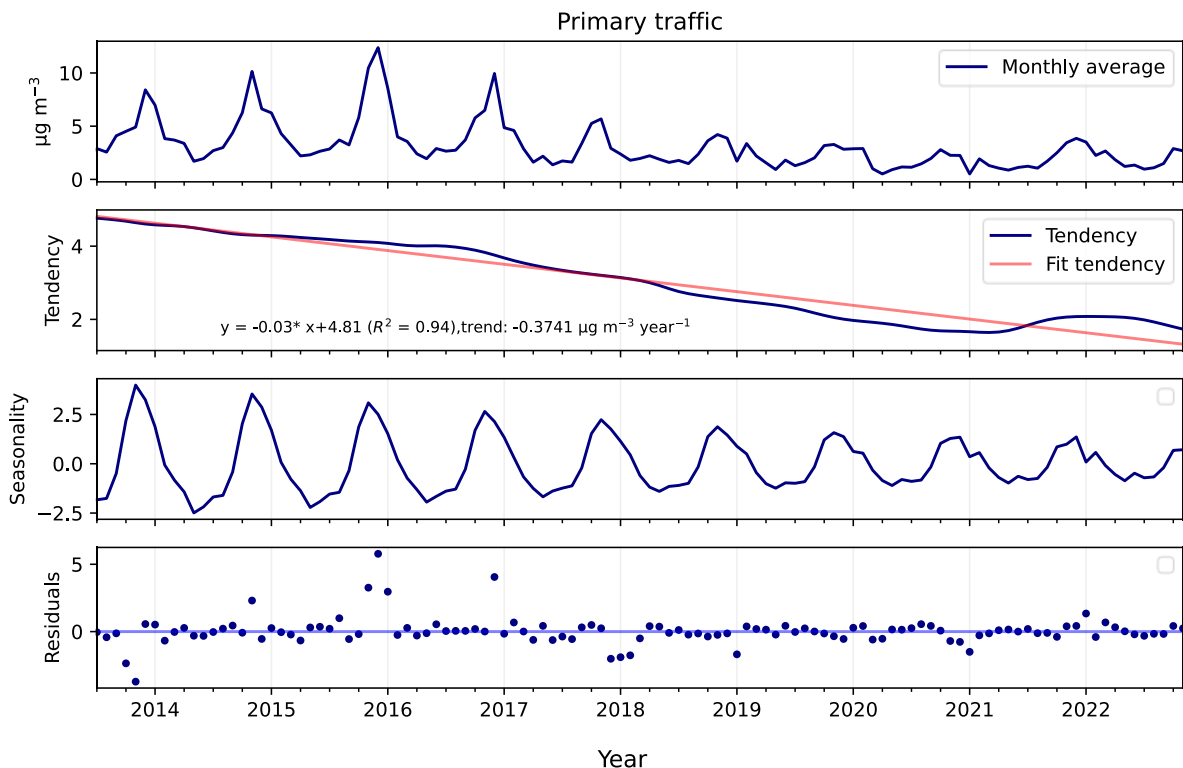


506
 507
 508 **Figure 8. Comparison between annual average PM_{10} emission inventory based on the quantity of wood sales (in grey)**
 509 **in the Grenoble metropolis and the yearly average PM_{10} concentrations from the PMF biomass burning factor (in**
 510 **green).**

511 Except for the year 2020, the annual average of biomass burning agreed with the emission inventory,
 512 demonstrating the consistency between the sources observed by the PMF model and the local inventory emission
 513 data. Since 2015, the Grenoble metropolis has set up an air-wood bonus to encourage households to renew their
 514 individual wood-burning appliance (fireplace or stove). It aims to replace all open fireplaces with closed
 515 appliances in October 2024. The downward trend of biomass burning concentration could then be considered as
 516 partly due to the implementation of dedicated action plans at the regional scale.

517 **3.3.4. Trends in traffic exhaust emissions**

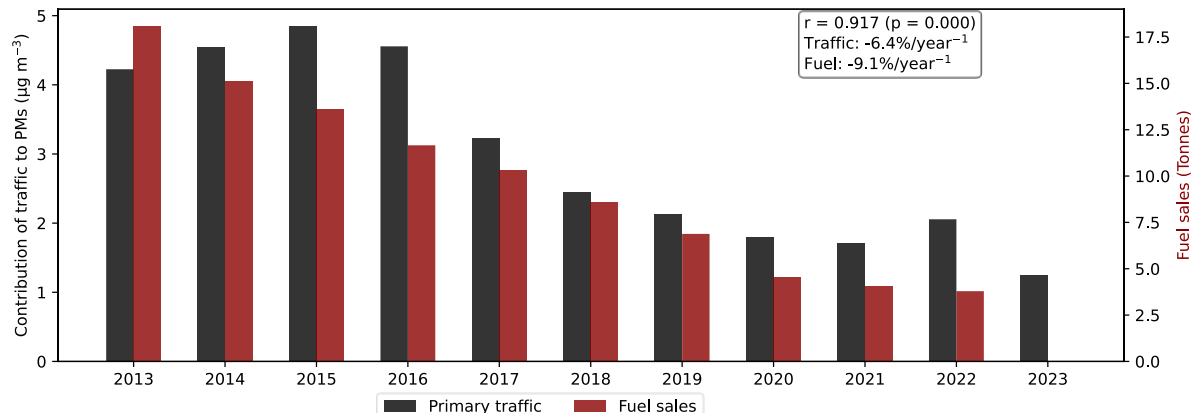
518 Similar to the time series of biomass burning concentrations, the traffic contribution was subjected to specific
 519 STL analysis (Figure 9). A significant downward trend of the concentrations of PM from traffic emission is
 520 detected with a reduction of $374 \text{ ng m}^{-3} \text{ yr}^{-1}$ ($12.9\% \text{ yr}^{-1}$) ($p\text{-value} << 0.01$). This reduction is almost 3 times larger
 521 than that of the biomass burning concentrations. Traffic concentration before 2017 also showed a clear seasonality
 522 with maxima in winter, which nearly disappeared from 2018 onward. It is striking that the same behaviors (strong
 523 downward trend and smoothing) are also observed for NO_x concentration, another indicator of traffic exhaust
 524 emission, which is also observed for NO_x seasonal patterns (see Supplement S6 and Figure S7). Residuals show
 525 extreme values in the same month as biomass burning in 2016 and 2017, matching the PM_{10} episode. The traffic
 526 trend closely follows a linear regression fit line, with $R^2 = 0.94$.



527
528 **Figure 9. The season-trend (STL) decomposition of PMF-derived traffic source**

529 The downward traffic trend observed in this study is consistent with another long-term study (2012-2020) of a
 530 rural site in France, which showed a traffic trend of $-6.5\% \text{ yr}^{-1}$ (58% total reduction) (Borlaza et al., 2022a). This
 531 is aligned with other results of fossil fuel black carbon in several rural sites in France (Font et al., 2025), or EC
 532 over many rural sites in Europe (Aas et al., 2024). Additionally, our result also agrees with other studies, like that
 533 by Pandolfi et al. (2016), which indicated a downward trend of traffic sources in an urban site in Spain, with a
 534 reduction of $5.6\% \text{ yr}^{-1}$ (56% total reduction), which is lower than that of our study. Finally, the trend of traffic
 535 emission to PM_{10} in 30 European countries was modeled as reported by Colette et al. (2021), showing a downward
 536 trend with a reduction from 2.3 to $3.5\% \text{ yr}^{-1}$ from 2000 to 2017. As for biomass burning, the Grenoble supersite
 537 seems then experiencing faster reductions in primary traffic PM loadings than most of others European cities.
 538 Furthermore, the PMF-derived traffic factor was compared to the local PM_{10} traffic emission inventory by fuel
 539 type (provided by Atmo AuRA), revealing very similar trends (Figure 10). In addition, this source is also
 540 compared to the PM_{10} emission by the transport sector (kilotonnes) over France, which was assessed from the
 541 emission inventory data of CITEPA (Figure S11), also confirming the concomitant reductions of traffic emissions
 542 and contributions to PM_{10} in ambient air.

543



544
545 **Figure 10. Comparison between annual average PM₁₀ emission inventory based on the quantity of fuel sale (red bar)**
546 **in the Grenoble metropolis and the yearly average PM₁₀ concentrations from the PMF-derived traffic source**
547 **contributions (black bar).**

548 This traffic trend may be separated into three parts. Between 2014 and 2016 with a slow decrease trend of -3% yr⁻¹; from 2016 to 2021, with an average reduction of 10% yr⁻¹, and a mild increasing trend of approximately 3% yr⁻¹ in the last three years of the study. The beginning of this increase coincides with the post-lockdown period, when 551 transportation activities were back to normal, resulting in a fairly similar contribution of traffic sources compared 552 to that in the pre-lockdown period.

553 Besides the implementation of the two versions of the Euro 6 emission standards (introduced in 2015 and 2018, 554 respectively), local emission abatement strategies decided by Grenoble municipality from 2016 onwards might be 555 the main drivers for the observed decreasing trends (City's low emission zone 556 <https://zfe.grenoblealpesmetropole.fr/> last assessed: 21/05/2025).

557 3.4. Trends in PM₁₀ OP sources

558 In this section, the sources of OP are assessed using regression techniques, which are presented in section 2.6. 559 The most appropriate model is selected based on characteristics of PMF-derived sources and OP_v, as shown in 560 section 3.4.1. Intrinsic OP derived from the best regression model, indicating the highest redox-active PM sources, 561 is presented in section 3.4.2. Finally, section 3.4.3 provides the trend of OP sources, highlighting which sources 562 are the drivers of OP trends.

563 3.4.1. Selection of the most appropriate model

564 Following the methodology exposed in Ngoc Thuy et al. (2024), the characteristics of the dataset, including 565 collinearity and heteroscedasticity, are tested in order to select a satisfactory inversion model for OP_{DTT} source 566 apportionment (SA) and OP_{AA} SA (Table S8). The OP SA can be applied for the 11-year PMF solution since the 567 source profiles have been demonstrated to be homogenous over the years. Consequently, the OP^m should be 568 substantially homogenous over the years (Ngoc Thuy et al., 2024), and it is unnecessary to perform the OP SA 569 for each year separately. The characteristic tests indicate that the weighted positive least squares (wPLS) and 570 weighted least squares (WLS) could be suitable models for both OP_{AA} and OP_{DTT} SA. The average accuracy 571 metrics of the testing dataset in 500 iteration runs (including R², RMSE, MAE) of wPLS and WLS were compared 572 to select the most appropriate model (Table S9). Finally, WLS was chosen due to the highest R² and lowest error 573 for both OP_{AA} and OP_{DTT} prediction. The comparison between observed and predicted OP_{AA} and OP_{DTT} showed

574 a good correlation between measured OP and WLS predicted OP, with $R^2 = 0.80$ and 0.70 for OP_{AA} and OP_{DTT} ,
575 respectively (Figure S12 and S13), with $n = 1570$ for OP_{AA} and OP_{DTT} .

576 **In addition, the study revealed good performance of Multiple Layer Perceptron (MLP) and Random Forest**
577 **(RF) for the training and testing datasets (Table S10).** These neural network models were overfitting the
578 results of OP SA for the 6 French sites tested in Ngoc Thuy et al. (2024) since the number of samples was
579 lower than 200 for individual sites. The present study confirmed the conclusion of Ngoc Thuy et al. (2024),
580 demonstrating that a higher number of samples improved the performance of the neural network model.
581 However, such non-linear models do not provide values for the intrinsic OP, which is basically the
582 regression slope of the regression. Since the objectives of MLP and RF are not to define a "slope" but to
583 better predict OP, therefore, the "slopes" of such models actually constantly vary with the input data to
584 ensure the best performance of the model. Since the OP intrinsic is not defined, these models cannot be
585 selected for the final results at this stage. **3.4.2. Intrinsic OP of PMF-derived sources**

586 The intrinsic OP of $1\mu\text{g}$ PM_{10} source ($OP^m \text{ nmol min}^{-1} \mu\text{g}^{-1}$) is investigated thanks to the WLS technique, resulting
587 in 500 values of OP^m for each source (Table 2 and Table S11). The anthropogenic sources, including biomass
588 burning, industrial, and traffic, have the dominant intrinsic OP_{DTT} and OP_{AA} , which is consistent with the study in
589 2017-2018 in Grenoble (Borlaza, 2021) and results obtained at other French sites (Ngoc Thuy et al., 2024; Weber
590 et al., 2021) and EU sites (Fadel et al., 2023; Veld et al., 2023). The different ranking of the intrinsic OP of the
591 sources according to the two assays is also aligned with previous results (Weber et al., 2021). While intrinsic
592 OP_{AA} of biomass burning is highest ($0.76 \text{ nmol min}^{-1} \mu\text{g}^{-1}$), followed by industrial ($0.48 \text{ nmol min}^{-1} \mu\text{g}^{-1}$) and
593 traffic ($0.38 \text{ nmol min}^{-1} \mu\text{g}^{-1}$), the order of intrinsic OP_{DTT} is industrial ($0.52 \text{ nmol min}^{-1} \mu\text{g}^{-1}$), traffic (0.38 nmol
594 $\text{min}^{-1} \mu\text{g}^{-1}$) and biomass burning ($0.14 \text{ nmol min}^{-1} \mu\text{g}^{-1}$). The intrinsic OP_{DTT} of biomass burning is also lower than
595 that of OP_{AA} , as reported by Borlaza et al. (Borlaza et al., 2021), suggesting the synergistic and antagonistic effects
596 between some elements, quinones, or bioaerosols, decreasing the overall intrinsic OP_{DTT} of this source
597 (Pietrogrande et al., 2022; Samake et al., 2017; Xiong et al., 2017).

598 The other anthropogenic sources, including nitrate-rich and sulfate-rich, have lower intrinsic OP than
599 anthropogenic sources associated with combustion (traffic and biomass burning), as reported by Daellenbach et
600 al. (2020). The natural sources have a negligible intrinsic OP (lower than $0.03 \text{ nmol min}^{-1} \mu\text{g}^{-1}$ for OP_{DTT} and 0.2
601 $\text{nmol min}^{-1} \mu\text{g}^{-1}$ for OP_{AA}). These findings highlight the high impact of the anthropogenic sources, verified for the
602 overall period 2013-2023.

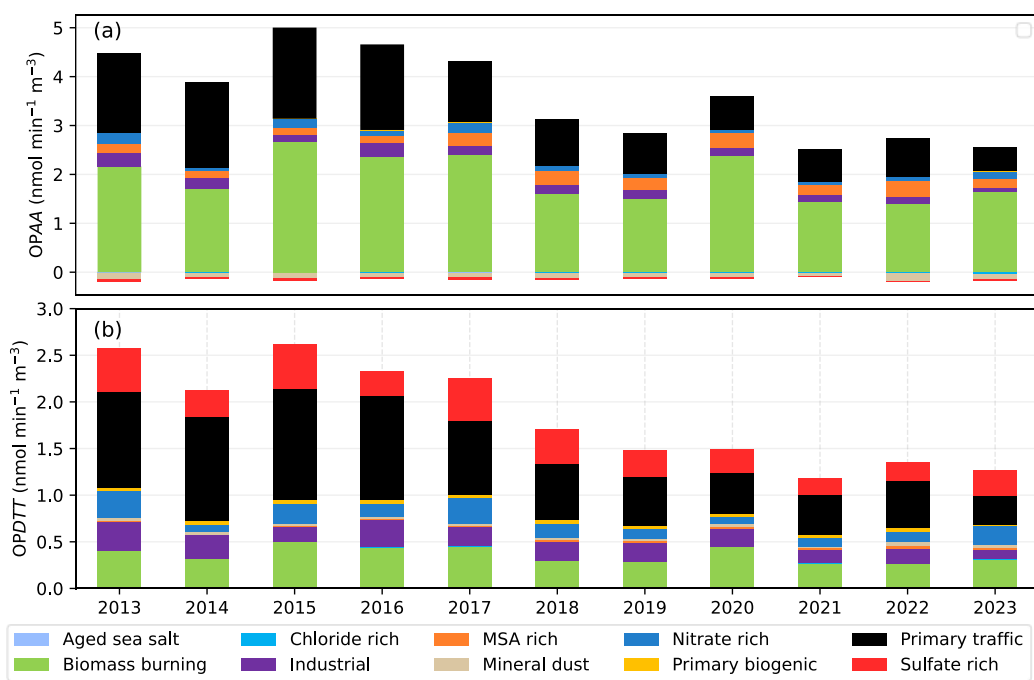
603 **Table 2. Intrinsic OP_{AA} and OP_{DTT} ($\text{nmol min}^{-1} \mu\text{g}^{-1}$) of PM_{10} sources (mean \pm std of 500 iterations)**

Source	OP_{AA}	OP_{DTT}
Aged sea salt	-0.02 ± 0.07	0.03 ± 0.02
Biomass burning	0.76 ± 0.13	0.14 ± 0.09
Chloride rich	-0.07 ± 0.09	0.01 ± 0.02
Industrial	0.48 ± 0.14	0.52 ± 0.08
MSA rich	0.20 ± 0.04	0.01 ± 0.02
Mineral dust	-0.03 ± 0.06	0.01 ± 0.02
Nitrate rich	0.09 ± 0.16	0.11 ± 0.12
Primary biogenic	0.00 ± 0.04	0.02 ± 0.03
Primary traffic	0.38 ± 0.10	0.24 ± 0.07
Sulfate rich	-0.01 ± 0.08	0.09 ± 0.04

604 **3.4.3. Trends in OP**

605 The trend of OP is first presented by the yearly average contribution of sources to OP_{AA} and OP_{DTT} (Figure 4),
 606 indicating a reduction of OP values over the years. Overall, the yearly average of the OP_{AA}^v and OP_{DTT}^v is
 607 decreasing and reached its lowest values in 2021 (2.41 and 1.17 $\text{nmol min}^{-1} \text{m}^{-3}$ for OP_{AA} and OP_{DTT} , respectively).
 608 From 2018 onward, both assays consistently exhibited lower OP^v values than in preceding years. Although OP^v
 609 is calculated using PM_{10} concentration, implying that a decrease in PM_{10} concentration generally reduces OP^v,
 610 the contribution of sources to OP is different from that of PM_{10} . While dust and sulfate-rich are dominantly
 611 contribute to PM_{10} , biomass burning is the most important contributor to OP_{AA} ($1.87 \pm 2.7 \text{ nmol min}^{-1} \text{m}^{-3}$), and
 612 primary traffic is commonly assessed as the largest contributor to OP_{DTT} ($0.71 \pm 0.70 \text{ nmol min}^{-1} \text{m}^{-3}$). The
 613 industrial mass contribution is 10 times lower than that of the sulfate-rich. However, industrial emissions appear
 614 to contribute much more to OP_{AA} and equally to OP_{DTT} than the sulfate-rich factor. This finding was also observed
 615 in 2017-2018 at the same site in Grenoble (Borlaza, 2021). This significant contribution of traffic and biomass
 616 burning over the years is more evident when considering relative contribution (Figure S15). These results again
 617 emphasize the importance of considering not only the mass concentration but also its redox activity in evaluating
 618 the potential adverse health effects of a source of PM.

619 In addition, the temporal evolution of OP_{AA} and OP_{DTT} did not exactly follow PM_{10} trends, especially for the
 620 period of 2016-2017 and 2019-2020. Regarding the period between 2016 and 2017, a dramatic increase in PM_{10}
 621 concentration is observed, principally due to the higher contribution of nitrate and sulfate-rich. On the other hand,
 622 OP_{AA} and OP_{DTT} values remained fairly unchanged between 2016 and 2017. Focus on 2019 and 2020, the PM
 623 concentration and OP^v values are identical (less than $0.001 \mu\text{g m}^{-3}$ and $\text{nmol min}^{-1} \text{m}^{-3}$ of difference, respectively),
 624 while OP_{AA}^v presents a remarkable difference ($\Delta = 0.8 \text{ nmol min}^{-1} \text{m}^{-3}$). Indeed, the discrepancy between 2019
 625 and 2020 in OP_{AA}^v is principally attributable to a higher contribution to biomass burning, which is the dominant
 626 driver of OP_{AA}^v . Overall, the downward trend of OP_{AA} and OP_{DTT} is different from PM_{10} , since the driven sources
 627 of OP and PM are different.



628 **Figure 11. Yearly average contribution of sources to (a) OP_{AA}^v and (b) OP_{DTT}^v**

629

630 The yearly average may not be properly representative of the trends of OP; therefore, a STL deconvolution was
631 performed for OP_{AA}^m and OP_{DTT}^m (Figures S16, S17, respectively) to investigate the trend of OP^m over the 11
632 years of the study. Indeed, considering the trend of the intrinsic OP^m confirms that the downward trend of some
633 sources leads to a change in the trend of OP_{AA}^m and OP_{DTT}^m .

634 An insignificant linear trend is observed for OP_{AA}^m (fit line: $R^2 = 0.4$, p-values << 0.01), yet its average intrinsic
635 activity still exhibits a decreasing value, with the annual mean falling by approximately $0.002 \text{ nmol min}^{-1} \text{ m}^{-3}$
636 (2.5 %) across the study period. Interestingly, the seasonality of OP_{AA}^m exactly matches the seasonality of
637 biomass-burning concentrations, pointing out that the high values of OP_{AA}^m in winter align with biomass-burning
638 activities. The trend line of OP_{AA}^m did not match the trend of biomass burning nor that of the traffic or industrial
639 emissions, suggesting the synergistic effect between sources, as well as the influence of the other sources outside
640 of the winter season, such as MSA-rich and primary biogenic, which get a high ranking of OP_{AA}^m (Table 2).

641 Conversely, the OP_{DTT}^m showed a significant downward trend ($R^2 = 0.6$, p-value << 0.01), with a reduction of 0.005
642 $\text{nmol min}^{-1} \mu\text{g}^{-1}$ (6.5%) across 11 years. The seasonality of OP_{DTT} is different from that of biomass burning and
643 OP_{AA}^m , since biomass burning is not the main driver of OP_{DTT} (only ranked third), indicating a lower influence of
644 this source on OP_{DTT}^m compared to OP_{AA}^m . Interestingly, a slight increase in OP_{DTT}^m from 2021 onward is also
645 observed, which is associated with PM_{10} and traffic, suggesting that traffic emission could be the main driver for
646 increasing PM_{10} concentration and OP_{DTT}^m from 2021. Overall, the relative decrease of OP_{DTT}^m exceeds that of
647 OP_{AA}^m could be explained by the 4th most important contributor to these OPs. All four leading contributors to
648 OP_{DTT}^m show significant reductions, whereas MSA-rich factor, one of the top four contributors to OP_{AA}^m , has an
649 increasing trend. These findings again underscore that trends in OP^m are governed by the evolution of the sources
650 most active in each assay. Thus, the decrease in the magnitude of the OP_m depends on how its dominant redox-
651 active sources evolve over time.

652 Considering the volume-based metrics (OP_v), a downward trend is detected for OP_{AA} and OP_{DTT} . PM_{10} decreased
653 by 3.9 % over the decade, which is consistently comparable to OP_{AA}^v (4.9 %) and OP_{DTT}^v (5.3 %). This good
654 agreement partially reflects the influence of the PM mass concentration since these OP_v values are calculated
655 using PM_{10} concentration. However, the slight difference in the relative downward trend could be related to the
656 most driven sources of OP and PM, as discussed above.

657 Finally, the impact of persistent inversion days on the OP^v is also investigated to assess the association between
658 the redox activity of PM sources and thermal inversion. A comparison of the source's contribution to OP^v (for
659 both AA and DTT) between the period with and without persistent inversions is carried out and shown in Figure
660 S14. The comparison confirms the larger increases in average OP_{AA} (85.1%) and OP_{DTT} (63.8 %) compared to
661 that of PM_{10} (39.6%) for the persistent inversion periods. The higher values of OP_{AA} and OP_{DTT} are related to the
662 larger increases in the contribution of local anthropogenic sources, with BB impacting most the OP_{AA} values while
663 traffic significantly influences OP_{DTT} . This result again highlights the potential effect of persistent inversion on
664 the PM_{10} source's contribution, but all the more of their redox-active properties, which could be associated with
665 the health-relevant metrics (Tassel et al., 2025 in progress).

666 Over the decade, anthropogenic sources have driven OP, with biomass burning impacting OP_{AA} and traffic/
667 industrial sources dominating OP_{DTT} . Frequent thermal inversion in Alpine valley strongly amplifies OP, which is
668 more significant than the mass of PM_{10} itself. Finally, OP_v and intrinsic OP trends over the decade do not align

669 with that of PM_{10} mass, emphasizing the need to prioritize redox-active components over the bulk PM_{10}
670 concentration in air quality policy.

671 **4. Conclusions**

672 Thanks to long-term PM_{10} observations with a detailed set of chemical markers, a comprehensive source
673 apportionment was performed to identify the evolution of PM_{10} sources in Grenoble (France). This is one of the
674 very few studies in Europe that could assess over 11 years of PM_{10} sources and the only study so far investigating
675 trends in PM_{10} -related OP. The trend of PM_{10} sources, especially anthropogenic sources such as biomass burning
676 and primary traffic, was evaluated and linked to the meteorology and emission reduction policies. In addition, the
677 trend of OP^m , OP^v , and sources of OP revealed that the trend of OP depends on the source that drives OP. The
678 analysis of these trends confirms the improvement of the air quality at the Grenoble supersite from 2013 to 2023,
679 and objectivates the main sources that are involved in their concentration' decrease.

680 Nevertheless, the following methodological limitations in this long-term study shall be kept in mind:

681 - Daily concentrations of metal elements were only analyzed for some periods (2013, 2017-2018, 2020-2021),
682 while the remaining data were derived from weekly sampling. An imputation technique was implemented to
683 impute daily concentrations. The PMF result demonstrated the stability of most chemical profiles at Grenoble
684 from 2013 to 2023, compared to those previously published (Borlaza et al., 2021), despite these uncertainties in
685 the imputed metal concentrations.

686 - The process of implementing such a PMF analysis strategy is not straightforward. A combined PMF approach
687 could be used for datasets with different time resolution (Via et al., 2023). This approach would allow combining
688 the 7-day and daily filter samples into a PMF without performing imputation.

689 - The lack of a secondary biogenic organic aerosol tracer in long-term observations prevents the identification of
690 the BSOA source, which could make up about 10% of the total mass of PM_{10} on a yearly average, as observed in
691 previous work at the site (Borlaza et al., 2021), which used 3-MBTCA and picnic acid for the yearly period of
692 observation.

693 Thanks to long-term PM_{10} observations with a detailed set of chemical markers, a comprehensive source
694 apportionment was performed to identify the evolution of PM_{10} sources in Grenoble (France). This is one of the
695 very few studies in Europe that could assess over 11 years of PM_{10} sources and the only study so far investigating
696 trends in PM_{10} -related OP. The trend of PM_{10} sources, especially anthropogenic sources such as biomass burning
697 and primary traffic, was evaluated and linked to the meteorology and emission reduction policies. In addition, the
698 trend of OP^m , OP^v , and sources of OP revealed that the trend of OP depends on the source that drives OP. The
699 analysis of these trends confirms the improvement of the air quality at the Grenoble supersite from 2013 to 2023,
700 and objectivates the main sources that are involved in their concentration' decrease.

701 Overall, a total of ten sources were identified, including aged sea salt, biomass burning, chloride-rich mineral
702 dust, MSA-rich, nitrate-rich, industrial, primary biogenic, and primary traffic. The source chemical profiles are
703 consistent with those presented in 2017-2018 (Borlaza et al., 2021), demonstrating that the sources of PM_{10} in
704 Grenoble were relatively stable during our study period. The trend of PM_{10} sources was investigated using STL
705 decomposition, which reveals a downward trend for all the PM_{10} sources over 11 years, especially for the
706 anthropogenic sources. Extending PMF outputs to oxidative potential apportionment showed that biomass
707 burning, traffic, and industrial emissions dominate redox activity in both the ascorbic acid (AA) and dithiothreitol

708 (DTT) assays. Trend analysis of volume- and mass-normalized OP metrics indicates that biomass burning governs
709 the long-term behavior of OP_{AA} . In contrast, traffic is the principal driver of OP_{DTT} assay, underscoring source-
710 specific control of PM_{10} OP in the Grenoble atmosphere.

711 Both of these anthropogenic sources, as well as their influences on PM_{10} OP, showed significant decreasing trends
712 concomitantly to the implementation of emission reduction strategies (both at the national and regional levels)
713 that should be reinforced to reach the goals of the European zero pollution action plan and the recently revised
714 Directive on ambient air quality (22024/2881/EU). The continuation of these measurements will take place in the
715 coming years, with this site being selected as one of the supersites for the new EU Air Quality directive.

716 **Data availability**

717 The datasets could be made available upon request by contacting the corresponding authors.

718 **Author contributions**

719 VDNT performed the source apportionment and the trend of sources, and the result visualisation. GU, JLJ
720 mentoring, supervision, validation of the methodology and results. RE, SD, CV, and AN contributed to data
721 acquisition (analytical investigation on samples) and data curation. OF, JLJ, and GU acquired funding for the
722 original PM sampling and analysis. VDNT wrote the original draft. All authors reviewed and edited the
723 manuscript.

724 **Competing interests**

725 The authors declare that they have no conflict of interest.

726 **Acknowledgment**

727 The authors would like to express their sincere gratitude to many people of the Air-O-Sol analytical platform at
728 IGE for sample management and chemical analyses. We gratefully acknowledge the personnel at Atmo AuRA
729 (C. Bret, C. Chabanis) for their support in conducting the dedicated sample collection and providing weekly metals
730 data.

731 **Financial support**

732 This study was partially funded by the French Ministry of Environment through its contributions to the CARA
733 program. Part of the project was also funded by Atmo AuRA (ensuring filter sampling and costs related to the
734 analyses of the elemental concentrations in the weekly samples. IGE contributed financially to the analyses of
735 ions. The extended analyses for the daily trace elements were funded by the QAMECS program from Ademe
736 (1662C0029).

737

738 **Reference**

739 Aas, W., Fagerli, H., Alastuey, A., Cavalli, F., Degorska, A., Feigenspan, S., Brenna, H., Gliß, J., Heinesen, D.,
740 Hueglin, C., Holubová, A., Jaffrezo, J.-L., Mortier, A., Murovec, M., Putaud, J.-P., Rüdiger, J., Simpson, D.,
741 Solberg, S., Tsyro, S., Tørseth, K., and Yttri, K. E.: Trends in Air Pollution in Europe, 2000–2019, *Aerosol and*
742 *Air Quality Research*, 24, 230237, <https://doi.org/10.4209/aaqr.230237>, 2024.

743 Allard, J., Chevrier, F., Laurent, J.-P., Coulaud, C., Paci, A., Jezek, I., Moenik, G., Brulfert, G., Besombes, J.-L.,
744 and Jaffrezo, J.-L.: Un système de mesure de température pour suivre l'influence de la stabilité atmosphérique sur
745 la qualité de l'air dans la vallée de l'Arve, *Météorologie*, 39, <https://doi.org/10.4267/2042/70368>, 2019.

746 Ayres, J. G., Borm, P., Cassee, F. R., Castranova, V., Donaldson, K., Ghio, A., Harrison, R. M., Hider, R., Kelly,
747 F., Kooter, I. M., Marano, F., Maynard, R. L., Mudway, I., Nel, A., Sioutas, C., Smith, S., Baeza-Squiban, A.,
748 Cho, A., Duggan, S., and Froines, J.: Evaluating the toxicity of airborne particulate matter and nanoparticles by
749 measuring oxidative stress potential - A workshop report and consensus statement, *Inhalation Toxicology*, 20, 75–
750 99, <https://doi.org/10.1080/08958370701665517>, 2008.

751 Azur, M. J., Stuart, E. A., Frangakis, C., and Leaf, P. J.: Multiple imputation by chained equations: what is it and
752 how does it work?, *International journal of methods in psychiatric research*, 20, 40–49,
753 <https://doi.org/10.1002/mps.329>, 2011.

754 Baduel, C., Voisin, D., and Jaffrezo, J.-L.: Water-soluble atmospheric HULIS in urban environments Water-
755 soluble atmospheric HULIS in urban environments Water-soluble atmospheric HULIS in urban environments,
756 *Chem. Phys. Discuss.*, 2009.

757 Baduel, C., Nozière, B., and Jaffrezo, J. L.: Summer/winter variability of the surfactants in aerosols from
758 Grenoble, France, *Atmospheric Environment*, 47, 413–420, <https://doi.org/10.1016/j.atmosenv.2011.10.040>,
759 2012.

760 Bates, J. T., Weber, R. J., Verma, V., Fang, T., Ivey, C., Liu, C., Sarnat, S. E., Chang, H. H., Mulholland, J. A.,
761 and Russell, A.: Source impact modeling of spatiotemporal trends in PM2.5 oxidative potential across the eastern
762 United States, *Atmospheric Environment*, 193, 158–167, <https://doi.org/10.1016/j.atmosenv.2018.08.055>, 2018.

763 Belis, C. A., Favez, O., Harrison, R. M., Larsen, B. R., Amato, F., El Haddad, I., Hopke, P. K., Nava, S., Paatero,
764 P., Prévôt, A., Quass, U., Vecchi, R., Viana, M., and European Commission (Eds.): European guide on air
765 pollution source apportionment with receptor models, Publications Office, Luxembourg, 1 pp.,
766 <https://doi.org/10.2788/9332>, 2014.

767 Belis, C. A., Karagulian, F., Amato, F., Almeida, M., Artaxo, P., Beddows, D. C. S., Bernardoni, V., Bove, M.
768 C., Carbone, S., Cesari, D., Contini, D., Cuccia, E., Diapouli, E., Eleftheriadis, K., Favez, O., El Haddad, I.,
769 Harrison, R. M., Hellebust, S., Hovorka, J., Jang, E., Jorquera, H., Kammermeier, T., Karl, M., Lucarelli, F.,
770 Mooibroek, D., Nava, S., Nøjgaard, J. K., Paatero, P., Pandolfi, M., Perrone, M. G., Petit, J. E., Pietrodangelo, A.,
771 Pokorná, P., Prati, P., Prevot, A. S. H., Quass, U., Querol, X., Saraga, D., Sciare, J., Sfetsos, A., Valli, G., Vecchi,
772 R., Vesterius, M., Yubero, E., and Hopke, P. K.: A new methodology to assess the performance and uncertainty
773 of source apportionment models II: The results of two European intercomparison exercises, *Atmospheric*
774 *Environment*, 123, 240–250, <https://doi.org/10.1016/j.atmosenv.2015.10.068>, 2015.

775 Borlaza: Disparities in particulate matter (PM10) origins and oxidative potential at a city scale (Grenoble, France)
776 - Part 2: Sources of PM10 oxidative potential using multiple linear regression analysis and the predictive
777 applicability of multilayer perceptron n, *Atmospheric Chemistry and Physics*, 21, 9719–9739,
778 <https://doi.org/10.5194/acp-21-9719-2021>, 2021.

779 Borlaza, L., Weber, S., Uzu, G., Jacob, V., Cañete, T., Micallef, S., Trébuchon, C., Slama, R., Favez, O., and
780 Jaffrezo, J.-L.: Disparities in particulate matter (PM10) origins and oxidative potential at a city scale (Grenoble,
781 France) - Part 1: Source apportionment at three neighbouring sites, *Atmospheric Chemistry and Physics*, 21, 5415–
782 5437, <https://doi.org/10.5194/acp-21-5415-2021>, 2021.

783 Borlaza, L., Weber, S., Marsal, A., Uzu, G., Jacob, V., Besombes, J. L., Chatain, M., Conil, S., and Jaffrezo, J.
784 L.: Nine-year trends of PM10 sources and oxidative potential in a rural background site in France, *Atmospheric*
785 *Chemistry and Physics*, 22, 8701–8723, <https://doi.org/10.5194/acp-22-8701-2022>, 2022a.

786 Borlaza, L., Weber, S., Marsal, A., Uzu, G., Jacob, V., Besombes, J. L., Chatain, M., Conil, S., and Jaffrezo, J.
787 L.: Nine-year trends of PM10 sources and oxidative potential in a rural background site in France, *Atmospheric*
788 *Chemistry and Physics*, 22, 8701–8723, <https://doi.org/10.5194/acp-22-8701-2022>, 2022b.

789 Borlaza-Lacoste, L., Mardoñez, V., Marsal, A., Hough, I., Dinh, N. T. V., Dominutti, P., Jaffrezo, J.-L., Alastuey,
790 A., Besombes, J.-L., Močnik, G., Moreno, I., Velarde, F., Gardon, J., Cornejo, A., Andrade, M., Laj, P., and Uzu,
791 G.: Oxidative potential of particulate matter and its association to respiratory health endpoints in high-altitude
792 cities in Bolivia, *Environmental Research*, 255, 119179, <https://doi.org/10.1016/j.envres.2024.119179>, 2024.

793 Brighty, A., Jacob, V., Uzu, G., Borlaza, L., Conil, S., Hueglin, C., Grange, S. K., Favez, O., Trébuchon, C., and
794 Jaffrezo, J. L.: Cellulose in atmospheric particulate matter at rural and urban sites across France and Switzerland,
795 *Atmospheric Chemistry and Physics*, 22, 6021–6043, <https://doi.org/10.5194/acp-22-6021-2022>, 2022.

796 Calas, A., Uzu, G., Martins, J. M. F., Voisin, Di., Spadini, L., Lacroix, T., and Jaffrezo, J. L.: The importance of
797 simulated lung fluid (SLF) extractions for a more relevant evaluation of the oxidative potential of particulate
798 matter, *Scientific Reports*, 7, 1–12, <https://doi.org/10.1038/s41598-017-11979-3>, 2017.

799 Calas, A., Uzu, G., Kelly, F. J., Houdier, S., Martins, J. M. F., Thomas, F., Molton, F., Charron, A., Dunster, C.,
800 Oliete, A., Jacob, V., Besombes, J. L., Chevrier, F., and Jaffrezo, J. L.: Comparison between five acellular
801 oxidative potential measurement assays performed with detailed chemistry on PM10 samples from the city of
802 Chamonix (France), *Atmospheric Chemistry and Physics*, 18, 7863–7875, <https://doi.org/10.5194/acp-18-7863-2018>, 2018.

804 Caporale, G. M., Gil-Alana, L. A., and Carmona-González, N.: Particulate matter 10 (PM10): persistence and
805 trends in eight European capitals, *Air Quality, Atmosphere and Health*, 14, 1097–1102,
806 <https://doi.org/10.1007/s11869-021-01002-0>, 2021.

807 Carbone, C., De Cesari, S., Mircea, M., Giulianelli, L., Finessi, E., Rinaldi, M., Fuzzi, S., Marinoni, A., Duchi, R.,
808 Perrino, C., Sargolini, T., Vardè, M., Sprovieri, F., Gobbi, G. P., Angelini, F., and Facchini, M. C.: Size-resolved
809 aerosol chemical composition over the Italian Peninsula during typical summer and winter conditions,
810 *Atmospheric Environment*, 44, 5269–5278, <https://doi.org/10.1016/j.atmosenv.2010.08.008>, 2010.

811 Colette, A., Solberg, S., Aas, W., and Walker, S.-E.: *Understanding Air Quality Trends in Europe*, 2021.

812 Craney, T. A. and Surles, J. G.: Model-dependent variance inflation factor cutoff values, *Quality Engineering*, 14,
813 391–403, <https://doi.org/10.1081/QEN-120001878>, 2002.

814 Daellenbach, K. R., Uzu, G., Jiang, J., Cassagnes, L.-E., Leni, Z., Vlachou, A., Stefenelli, G., Canonaco, F.,
815 Weber, S., Segers, A., and Sources, al: Sources of particulate-matter air pollution and its oxidative potential in
816 Europe of particulate-matter air pollution and its oxidative potential in Europe, *Nature*, 587,
817 <https://doi.org/10.1038/s41586-020-2902-8>; 2020.

818 Dominutti, P. A., Borlaza, L., Sauvain, J. J., Thuy, V. D. N., Houdier, S., Suarez, G., Jaffrezo, J. L., Tobin, S.,
819 Trébuchon, C., Socquet, S., Moussu, E., Mary, G., and Uzu, G.: Source apportionment of oxidative potential
820 depends on the choice of the assay: insights into 5 protocols comparison and implications for mitigation measures,
821 *Environmental Science: Atmospheres*, <https://doi.org/10.1039/d3ea00007a>, 2023.

822 Ducret-stich, R. E. and Tsai, M.: RESEARCH ARTICLE PM 10 source apportionment in a Swiss Alpine valley
823 impacted by highway traffic, 6496–6508, <https://doi.org/10.1007/s11356-013-1682-1>, 2013.

824 European committee for standardization: Ambient air - Determination of the concentration of levoglucosan -
825 Chromatographic method, CEN-CENELEC Management Centre, 2024.

826 Fadel, M., Courcot, D., Delmaire, G., Roussel, G., Afif, C., and Ledoux, F.: Source apportionment of PM2.5
827 oxidative potential in an East Mediterranean site, *Science of the Total Environment*, 900,
828 <https://doi.org/10.1016/j.scitotenv.2023.165843>, 2023.

829 Favez, O., El Haddad, I., Piot, C., Boréave, A., Abidi, E., Marchand, N., Jaffrezo, J. L., Besombes, J. L.,
830 Personnaz, M. B., Sciare, J., Wortham, H., George, C., and D'Anna, B.: Inter-comparison of source apportionment

831 models for the estimation of wood burning aerosols during wintertime in an Alpine city (Grenoble, France),
832 Atmospheric Chemistry and Physics, 10, 5295–5314, <https://doi.org/10.5194/acp-10-5295-2010>, 2010.

833 Favez, O., Weber, S., Petit, J. E., Alleman, L. Y., Albinet, A., Riffault, V., Chazeau, B., Amodeo, T., Salameh,
834 D., Zhang, Y., Srivastava, D., Samaké, A., Aujay-Plouzeau, R., Papin, A., Bonnaire, N., Boullanger, C., Chatain,
835 M., Chevrier, F., Detournay, A., Dominik-Sègue, M., Falhun, R., Garbin, C., Ghersi, V., Grignion, G.,
836 Levigoureux, G., Pontet, S., Rangognio, J., Zhang, S., Besombes, J. L., Conil, S., Uzu, G., Savarino, J., Marchand,
837 N., Gros, V., Marchand, C., Jaffrezo, J. L., and Leoz-Garziandia, E.: Overview of the French operational network
838 for in situ observation of PM chemical composition and sources in urban environments (CARA program),
839 Atmosphere, 12, <https://doi.org/10.3390/atmos12020207>, 2021.

840 Font, A., Ciupek, K., Butterfield, D., and Fuller, G. W.: Long-term trends in particulate matter from wood burning
841 in the United Kingdom: Dependence on weather and social factors, Environmental Pollution, 314, 120105,
842 <https://doi.org/10.1016/j.envpol.2022.120105>, 2022.

843 Font, A., F. De Brito, J., Riffault, V., Conil, S., Jaffrezo, J.-L., and Bourin, A.: Do rural background sites capture
844 changes in primary PM_{2.5} emissions at the national scale? Recent trends in PM_{2.5} and its main components in
845 metropolitan France., , <https://doi.org/10.5194/egusphere-egu25-10935>, 2025.

846 Fuzzi, S., Baltensperger, U., Carslaw, K., Decesari, S., Denier Van Der Gon, H., Facchini, M. C., Fowler, D.,
847 Koren, I., Langford, B., Lohmann, U., Nemitz, E., Pandis, S., Riipinen, I., Rudich, Y., Schaap, M., Slowik, J. G.,
848 Spracklen, D. V., Vignati, E., Wild, M., Williams, M., and Gilardoni, S.: Particulate matter, air quality and climate:
849 Lessons learned and future needs, Atmospheric Chemistry and Physics, 15, 8217–8299,
850 <https://doi.org/10.5194/acp-15-8217-2015>, 2015.

851 Gama, C., Monteiro, A., Pio, C., Miranda, A. I., Baldasano, J. M., and Tchepel, O.: Temporal patterns and trends
852 of particulate matter over Portugal: a long-term analysis of background concentrations, Air Quality, Atmosphere
853 and Health, 11, 397–407, <https://doi.org/10.1007/s11869-018-0546-8>, 2018.

854 Gary Norris, Rachelle Duvall, Steve Brown, and Song Bai: EPA Positive Matrix Factorization (PMF) 5.0
855 Fundamentals and User Guide, 2014.

856 Gianini, M. F. D., Fischer, A., Gehrig, R., Ulrich, A., Wichser, A., Piot, C., Besombes, J. L., and Hueglin, C.:
857 Comparative source apportionment of PM₁₀ in Switzerland for 2008/2009 and 1998/1999 by Positive Matrix
858 Factorisation, Atmospheric Environment, 54, 149–158, <https://doi.org/10.1016/j.atmosenv.2012.02.036>, 2012.

859 Glojek, K., Močnik, G., Alas, H. D. C., Cuesta-Mosquera, A., Drinovec, L., Gregorič, A., Ogrin, M., Weinhold,
860 K., Ježek, I., Müller, T., Rigler, M., Remškar, M., Van Pinxteren, D., Herrmann, H., Ristorini, M., Merkel, M.,
861 Markelj, M., and Wiedensohler, A.: The impact of temperature inversions on black carbon and particle mass
862 concentrations in a mountainous area, Atmospheric Chemistry and Physics, 22, 5577–5601,
863 <https://doi.org/10.5194/acp-22-5577-2022>, 2022.

864 Glojek, K., Thuy, V. D. N., Weber, S., Uzu, G., Manousakas, M., Elazzouzi, R., Džepina, K., Darfeuil, S., Ginot,
865 P., Jaffrezo, J. L., Žabkar, R., Turšič, J., Podkoritnik, A., and Močnik, G.: Annual variation of source contributions
866 to PM₁₀ and oxidative potential in a mountainous area with traffic, biomass burning, cement-plant and biogenic
867 influences, Environment International, 189, 108787, <https://doi.org/10.1016/j.envint.2024.108787>, 2024.

868 Goldfeld, S. M. and Quandt, R. E.: Some Tests for Homoscedasticity Author (s): Stephen M. Goldfeld and
869 Richard E. Quandt Source: Journal of the American Statistical Association, Jun., 1965, Vol. 60, No. 310
870 Published by: Taylor & Francis, Ltd. on behalf of the American Statistical Association, 60, 539–547, 1965.

872 Grantz, D. A., Garner, J. H. B., and Johnson, D. W.: Ecological effects of particulate matter, Environment
873 International, 29, 213–239, [https://doi.org/10.1016/S0160-4120\(02\)00181-2](https://doi.org/10.1016/S0160-4120(02)00181-2), 2003.

874 Hopke, P. K.: Review of receptor modeling methods for source apportionment, Journal of the Air and Waste
875 Management Association, 66, 237–259, <https://doi.org/10.1080/10962247.2016.1140693>, 2016.

876 Hopke, P. K., Dai, Q., Li, L., and Feng, Y.: Global review of recent source apportionments for airborne particulate
877 matter, Science of The Total Environment, 740, 140091, <https://doi.org/10.1016/j.scitotenv.2020.140091>, 2020.

878 Largeron, Y. and Staquet, C.: Persistent inversion dynamics and wintertime PM10 air pollution in Alpine valleys,
879 *Atmospheric Environment*, 135, 92–108, <https://doi.org/10.1016/j.atmosenv.2016.03.045>, 2016.

880 Li, Xia, T., and Nel, A. E.: The role of oxidative stress in ambient particulate matter-induced lung diseases and its
881 implications in the toxicity of engineered nanoparticles, *Free Radical Biology and Medicine*, 44, 1689–1699,
882 <https://doi.org/10.1016/j.freeradbiomed.2008.01.028>, 2008.

883 Li, J., Chen, B., de la Campa, A. M. S., Alastuey, A., Querol, X., and de la Rosa, J. D.: 2005–2014 trends of PM10
884 source contributions in an industrialized area of southern Spain, *Environmental Pollution*, 236, 570–579,
885 <https://doi.org/10.1016/j.envpol.2018.01.101>, 2018.

886 Lodovici, M. and Bigagli, E.: Oxidative stress and air pollution exposure, *Journal of Toxicology*, 2011,
887 <https://doi.org/10.1155/2011/487074>, 2011.

888 Mudway, I. S., Kelly, F. J., and Holgate, S. T.: Oxidative stress in air pollution research, *Free Radical Biology
889 and Medicine*, 151, 2–6, <https://doi.org/10.1016/j.freeradbiomed.2020.04.031>, 2020.

890 Nelin, T. D., Joseph, A. M., Gorr, M. W., and Wold, L. E.: Direct and indirect effects of particulate matter on the
891 cardiovascular system, *Toxicology Letters*, 208, 293–299, <https://doi.org/10.1016/j.toxlet.2011.11.008>, 2012.

892 Ngoc Thuy, V. D., Jaffrezo, J.-L., Hough, I., Dominutti, P. A., Salque Moreton, G., Gille, G., Francony, F., Patron-
893 Anquez, A., Favez, O., and Uzu, G.: Unveiling the optimal regression model for source apportionment of the
894 oxidative potential of PM₁₀, *Atmospheric Chemistry and Physics*, 24, 7261–7282, <https://doi.org/10.5194/acp-24-7261-2024>, 2024.

896 O'Brien, R. M.: A caution regarding rules of thumb for variance inflation factors, *Quality and Quantity*, 41, 673–
897 690, <https://doi.org/10.1007/s11135-006-9018-6>, 2007.

898 Paatero, P. and Tappert, U.: Positive matrix factorization: A non-negative factor model with optimal utilization
899 of error estimates of data values, *Environmetrics*, <https://doi.org/10.1002/env.3170050203>, 1994.

900 Pandolfi, M., Alastuey, A., Pérez, N., Reche, C., Castro, I., Shatalov, V., and Querol, X.: Trends analysis of PM
901 source contributions and chemical tracers in NE Spain during 2004–2014: A multi-exponential approach,
902 *Atmospheric Chemistry and Physics*, 16, 11787–11805, <https://doi.org/10.5194/acp-16-11787-2016>, 2016.

903 Pietrodangelo, A., Bove, M. C., Forello, A. C., Crova, F., Bigi, A., Brattich, E., Riccio, A., Becagli, S., Bertinetti,
904 S., Calzolai, G., Canepari, S., Cappelletti, D., Catrambone, M., Cesari, D., Colombi, C., Contini, D., Cuccia, E.,
905 De Gennaro, G., Genga, A., Ielpo, P., Lucarelli, F., Malandrino, M., Masiol, M., Massabò, D., Perrino, C., Prati,
906 P., Siciliano, T., Tositti, L., Venturini, E., and Vecchi, R.: A PM10 chemically characterized nation-wide dataset
907 for Italy. Geographical influence on urban air pollution and source apportionment, *Science of The Total
908 Environment*, 908, 167891, <https://doi.org/10.1016/j.scitotenv.2023.167891>, 2024.

909 Pietrogrande, M. C., Romanato, L., and Russo, M.: Synergistic and Antagonistic Effects of Aerosol Components
910 on Its Oxidative Potential as Predictor of Particle Toxicity, *Toxics*, 10, <https://doi.org/10.3390/toxics10040196>,
911 2022.

912 Pope, C. A. and Dockery, D. W.: Health effects of fine particulate air pollution: Lines that connect, *Journal of the
913 Air and Waste Management Association*, 56, 709–742, <https://doi.org/10.1080/10473289.2006.10464485>, 2006.

914 Rao, X., Zhong, J., Brook, R. D., and Rajagopalan, S.: Effect of Particulate Matter Air Pollution on Cardiovascular
915 Oxidative Stress Pathways, Antioxidants and Redox Signaling, 28, 797–818,
916 <https://doi.org/10.1089/ars.2017.7394>, 2018.

917 Robert B Cleveland, William S. Cleveland, Jean E. McRae, and Irma Terpenning: STL: A Seasonal-Trend
918 decomposition Procedure Based on Loess, 1990.

919 Rosenblad, A.: The Concise Encyclopedia of Statistics, 867–868 pp.,
920 <https://doi.org/10.1080/02664760903075614>, 2011.

921 Samake, A., Uzu, G., Martins, J. M. F., Calas, A., Vince, E., Parat, S., and Jaffrezo, J. L.: The unexpected role of
922 bioaerosols in the Oxidative Potential of PM, *Scientific Reports*, 7, <https://doi.org/10.1038/s41598-017-11178-0>,
923 2017.

924 Samaké, A., Jaffrezo, J. L., Favez, O., Weber, S., Jacob, V., Canete, T., Albinet, A., Charron, A., Riffault, V.,
925 Perdrix, E., Waked, A., Golly, B., Salameh, D., Chevrier, F., Miguel Oliveira, D., Besombes, J. L., Martins, J. M.
926 F., Bonnaire, N., Conil, S., Guillaud, G., Mesbah, B., Rocq, B., Robic, P. Y., Hulin, A., Le Meur, S.,
927 Descheemaeker, M., Chretien, E., Marchand, N., and Uzu, G.: Arabitol, mannitol, and glucose as tracers of
928 primary biogenic organic aerosol: The influence of environmental factors on ambient air concentrations and
929 spatial distribution over France, *Atmospheric Chemistry and Physics*, 19, 11013–11030,
930 <https://doi.org/10.5194/acp-19-11013-2019>, 2019a.

931 Samaké, A., Jaffrezo, J. L., Favez, O., Weber, S., Jacob, V., Albinet, A., Riffault, V., Perdrix, E., Waked, A.,
932 Golly, B., Salameh, D., Chevrier, F., Miguel Oliveira, D., Bonnaire, N., Besombes, J. L., Martins, J. M. F., Conil,
933 S., Guillaud, G., Mesbah, B., Rocq, B., Robic, P. Y., Hulin, A., Le Meur, S., Descheemaeker, M., Chretien, E.,
934 Marchand, N., and Uzu, G.: Polyols and glucose particulate species as tracers of primary biogenic organic aerosols
935 at 28 French sites, *Atmospheric Chemistry and Physics*, 19, 3357–3374, <https://doi.org/10.5194/acp-19-3357-2019>, 2019b.

936 937 Seabold, S. and Perktold, J.: Statsmodels: Econometric and statistical modeling with python, in: 9th Python in
938 Science Conference, 2010.

939 Srivastava, D., Tomaz, S., Favez, O., Lanzafame, G. M., Golly, B., Besombes, J. L., Alleman, L. Y., Jaffrezo, J.
940 L., Jacob, V., Perraudin, E., Villenave, E., and Albinet, A.: Speciation of organic fraction does matter for source
941 apportionment. Part 1: A one-year campaign in Grenoble (France), *Science of the Total Environment*, 624, 1598–
942 1611, <https://doi.org/10.1016/j.scitotenv.2017.12.135>, 2018.

943 Tomaz, S., Shahpoury, P., Jaffrezo, J. L., Lammel, G., Perraudin, E., Villenave, E., and Albinet, A.: One-year
944 study of polycyclic aromatic compounds at an urban site in Grenoble (France): Seasonal variations, gas/particle
945 partitioning and cancer risk estimation, *Science of the Total Environment*, 565, 1071–1083,
946 <https://doi.org/10.1016/j.scitotenv.2016.05.137>, 2016.

947 Tomaz, S., Jaffrezo, J. L., Favez, O., Perraudin, E., Villenave, E., and Albinet, A.: Sources and atmospheric
948 chemistry of oxy- and nitro-PAHs in the ambient air of Grenoble (France), *Atmospheric Environment*, 161, 144–
949 154, <https://doi.org/10.1016/j.atmosenv.2017.04.042>, 2017.

950 Veld, M. in 't, Pandolfi, M., Amato, F., Pérez, N., Reche, C., Dominutti, P., Jaffrezo, J., Alastuey, A., Querol, X.,
951 and Uzu, G.: Discovering oxidative potential (OP) drivers of atmospheric PM10, PM2.5, and PM1 simultaneously
952 in North-Eastern Spain, *Science of the Total Environment*, 857, <https://doi.org/10.1016/j.scitotenv.2022.159386>,
953 2023.

954 Viana, M., Yus-Díez, J., Canonaco, F., Petit, J. E., Hopke, P., Reche, C., Pandolfi, M., Ivančić, M., Rigler, M.,
955 Prevôt, A. S. H., Querol, X., Alastuey, A., and Minguillón, M. C.: Towards a better understanding of fine PM
956 sources: Online and offline datasets combination in a single PMF, *Environment International*, 177,
957 <https://doi.org/10.1016/j.envint.2023.108006>, 2023.

958 Viana, M., Kuhlbusch, T. A. J., Querol, X., Alastuey, A., Harrison, R. M., Hopke, P. K., Winiwarter, W., Vallius,
959 M., Szidat, S., Prévôt, A. S. H., Hueglin, C., Bloemen, H., Wåhlin, P., Vecchi, R., Miranda, A. I., Kasper-Giebl,
960 A., Maenhaut, W., and Hitzenberger, R.: Source apportionment of particulate matter in Europe: A review of
961 methods and results, <https://doi.org/10.1016/j.jaerosci.2008.05.007>, 2008.

962 Vida, M., Foret, G., Siour, G., Coman, A., Weber, S., Favez, O., Jaffrezo, J. L., Pontet, S., Mesbah, B., Gille, G.,
963 Zhang, S., Chevrier, F., Pallares, C., Uzu, G., and Beekmann, M.: Oxidative potential modelling of PM10: a 2-
964 year study over France, ACDP, 2024.

965 Waked, A., Favez, O., Alleman, L. Y., Piot, C., Petit, J. E., Delaunay, T., Verlinden, E., Golly, B., Besombes, J.
966 L., Jaffrezo, J. L., and Leoz-Garziandia, E.: Source apportionment of PM10 in a north-western Europe regional
967 urban background site (Lens, France) using positive matrix factorization and including primary biogenic
968 emissions, *Atmospheric Chemistry and Physics*, 14, 3325–3346, <https://doi.org/10.5194/acp-14-3325-2014>, 2014.

969 Weber, S., Uzu, G., Calas, A., Chevrier, F., Besombes, J. L., Charron, A., Salameh, D., Ježek, I., Močnik, G., and
970 Jaffrezo, J. L.: An apportionment method for the oxidative potential of atmospheric particulate matter sources:
971 Application to a one-year study in Chamonix, France, *Atmospheric Chemistry and Physics*, 18, 9617–9629,
972 <https://doi.org/10.5194/acp-18-9617-2018>, 2018.

973 Weber, S., Salameh, D., Albinet, A., Alleman, L. Y., Waked, A., Besombes, J.-L., Jacob, V., Guillaud, G.,
974 Meshbah, B., Rocq, B., Hulin, A., Dominik-Sègue, M., Chrétien, E., Jaffrezo, J.-L., and Favez, O.: Comparison
975 of PM10 Sources Profiles at 15 French Sites Using a Harmonized Constrained Positive Matrix Factorization
976 Approach, *Atmosphere*, 10, 310, <https://doi.org/10.3390/atmos10060310>, 2019.

977 Weber, S., Uzu, G., Favez, O., Borlaza, L., Calas, A., Salameh, D., Chevrier, F., Allard, J., Besombes, J. L.,
978 Albinet, A., Pontet, S., Mesbah, B., Gille, G., Zhang, S., Pallares, C., Leoz-Garziandia, E., and Jaffrezo, J. L.:
979 Source apportionment of atmospheric PM10 oxidative potential: Synthesis of 15 year-round urban datasets in
980 France, *Atmospheric Chemistry and Physics*, 21, 11353–11378, <https://doi.org/10.5194/acp-21-11353-2021>,
981 2021.

982 Xiong, Q., Yu, H., Wang, R., Wei, J., and Verma, V.: Rethinking Dithiothreitol-Based Particulate Matter
983 Oxidative Potential: Measuring Dithiothreitol Consumption versus Reactive Oxygen Species Generation,
984 *Environmental Science and Technology*, 51, 6507–6514, <https://doi.org/10.1021/acs.est.7b01272>, 2017.

985 Yttri, K. E., Canonaco, F., Eckhardt, S., Evangelou, N., Fiebig, M., Gundersen, H., Hjellbrekke, A. G., Myhre,
986 C. L., Platt, S. M., Prevot, A. S. H., Simpson, D., Solberg, S., Surratt, J., Tørseth, K., Uggerud, H., Vadset, M.,
987 Wan, X., and Aas, W.: Trends, composition, and sources of carbonaceous aerosol at the Birkenes Observatory,
988 northern Europe, 2001–2018, *Atmospheric Chemistry and Physics*, 21, 7149–7170, <https://doi.org/10.5194/acp-21-7149-2021>, 2021.

990